ASRC Procedia
Global Perspectives in Science and Scholarship
Florida, USA

Volume: 1; **Issue:** 1
Pages: 1603– 1635
Published: 29 April 2025

open access

1st Global Research and Innovation Conference 2025,

April 20–24, 2025, Florida, USA

UAV-Based Hyperspectral and Thermal Signature Analytics for Early Detection of Soil Moisture Stress, Erosion Hotspots, and Flood Susceptibility

Ratul Debnath[1];

[1]. Graduate GIS Assistant, Sam Houston State University, Huntsville, TX, USA;
Email: ratuldebnathgis@gmail.com

Doi: 10.63125/c2vtn214
Peer-review under responsibility of the organizing committee of GRIC, 2025

Abstract

This study addresses the problem that soil moisture stress, erosion initiation, and localized flood exposure emerge at micro-scales that routine monitoring misses, delaying mitigation. The purpose was to test whether UAV-based hyperspectral and thermal signature analytics can deliver defensible early detection of soil moisture stress and improve erosion hotspot and flood susceptibility mapping using a quantitative, cross-sectional, case-based design. Across cloud and enterprise GIS deployment cases, the sample included 210 spatial zones within the case-study area, with five-point Likert composites for Soil Moisture Stress (SMS), Erosion Hotspot Concern (EHC), and Flood Susceptibility Perception (FSP). Key predictors were a hyperspectral moisture proxy (HSI_MoistureIndex), local thermal anomaly (TH_Anomaly), and terrain and hydrologic controls (slope, flow accumulation, distance to channel, and elevation). The analysis plan used descriptive statistics, Cronbach's alpha, Pearson correlations, multivariate regression with sensor-fusion model comparison, risk-class summaries, hotspot agreement (Jaccard), and robustness checks. Results indicated moderate-to-high perceived risk (SMS M=3.62, SD=0.71; EHC M=3.48, SD=0.76; FSP M=3.55, SD=0.74) and strong construct reliability (alpha=0.86, 0.83, and 0.88). SMS increased with TH_Anomaly (r=0.58, p<.001) and decreased with HSI_MoistureIndex (r=-0.52, p<.001). Regression confirmed a fusion gain: the fused stress model achieved Adj. R^2=0.58 and RMSE=0.44, outperforming hyperspectral-only (Adj. R^2=0.42, RMSE=0.56) and thermal-only (Adj. R^2=0.46, RMSE=0.53), with significant effects for TH_Anomaly (beta=0.41) and HSI_MoistureIndex (beta=-0.36). Erosion modeling achieved Adj. R^2=0.54 with flow accumulation and slope as primary drivers, and flood susceptibility improved from Adj. R^2=0.55 (terrain only) to 0.62 when thermal information was added. Spatial validation showed strong agreement for stress versus thermal hotspots (68% overlap; J=0.52) and flood susceptibility versus flow corridors (71% overlap; J=0.55), while sensitivity tests reduced the fused model from Adj. R^2=0.58 to 0.49 without TH_Anomaly and to 0.50 without HSI_MoistureIndex. High-risk classes covered 22 to 28% of zones and consistently aligned with Likert means above 4.0. Implications are that sensor-fusion UAV analytics, operationalized through cloud and enterprise workflows, can support earlier irrigation triage, prioritized erosion control in convergent high-slope zones, and more defensible flood preparedness zoning with auditable quantitative evidence.

Keywords

UAV Sensor Fusion, Hyperspectral Imaging, Thermal Infrared Anomaly, Soil Moisture Stress, Erosion And Flood Susceptibility Mapping;

INTRODUCTION

Unmanned aerial vehicles (UAVs) are airborne platforms operated remotely or autonomously that carry sensors to acquire georeferenced observations at spatial and temporal resolutions difficult to achieve using many satellite or crewed-aircraft workflows. In environmental monitoring, UAV value comes from controllable altitude, flexible revisit timing, and the ability to collect data at centimeter-to-decimeter ground sampling distances while targeting specific land units such as fields, embankments, riparian corridors, and unstable slopes (Baluja et al., 2012). In addition, Hyperspectral remote sensing refers to the measurement of reflected radiation in many narrow, contiguous spectral bands, usually spanning the visible, near-infrared, and sometimes shortwave infrared regions (Sadeghi et al., 2017). Such dense spectral sampling allows material and process discrimination based on absorption features and subtle spectral shape changes that are not resolved by broad multispectral bands (Pourghasemi et al., 2018). Thermal infrared (TIR) remote sensing measures emitted radiance related to land surface temperature, which is closely tied to surface energy partitioning, soil evaporation, and plant transpiration under given meteorological conditions (Allen et al., 2007).

Figure 1: UAV Hyperspectral–Thermal Workflow for Soil Moisture, Erosion, and Flood Risk

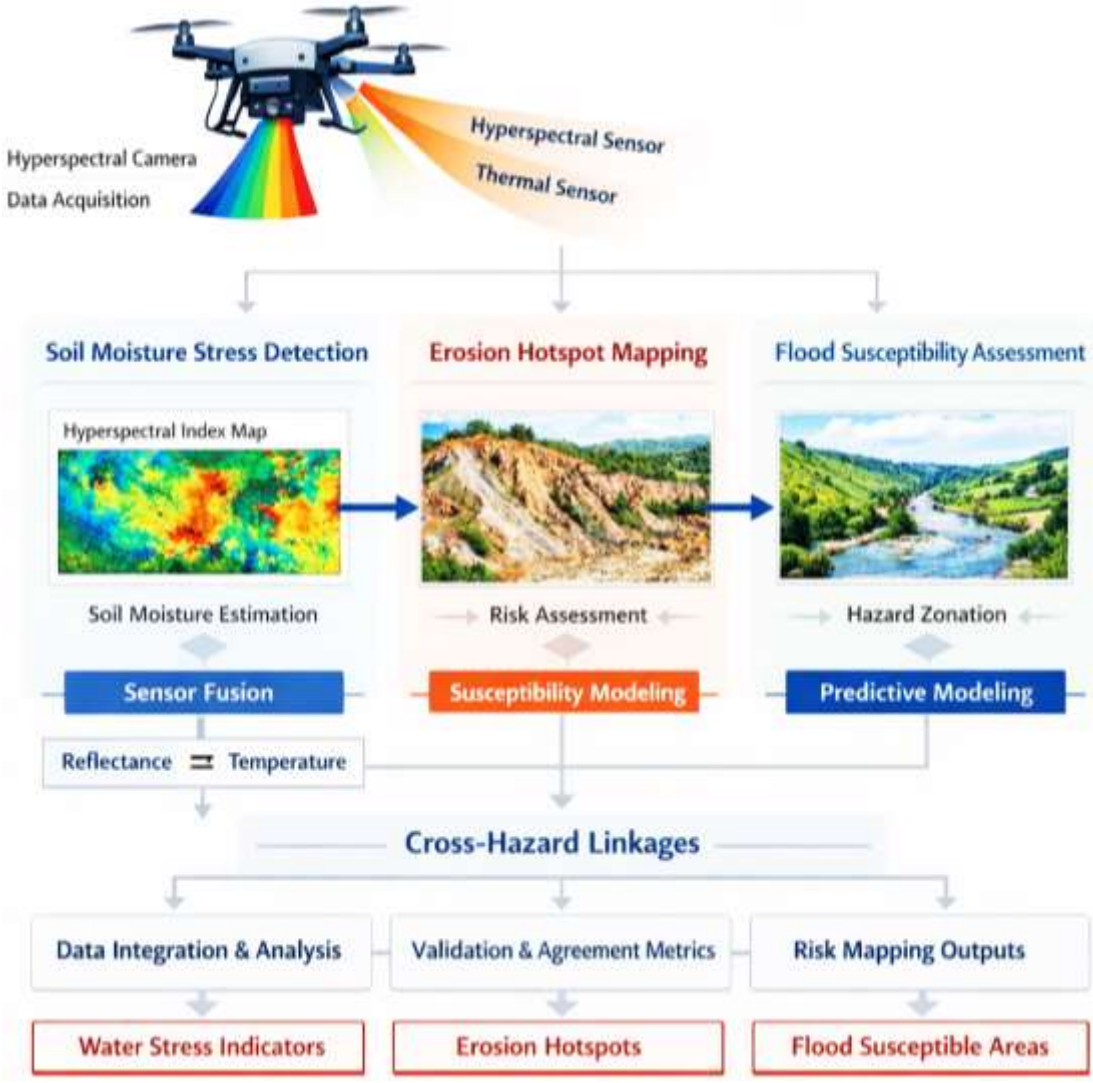

When hyperspectral and thermal measurements are acquired from UAVs, they can represent complementary views of land–surface condition: hyperspectral reflectance responds to pigment/water/structure and soil optical properties, while thermal patterns respond to aerodynamic–radiative forcing and moisture constraints through temperature and energy balance behavior (Santesteban et al., 2017). In applied hydrology and soil science, soil moisture stress is commonly

treated as a condition where water availability constrains biophysical function (e.g., reduced transpiration cooling and altered spectral response), and it can be examined through indices or modeled relationships linking observed spectral/thermal variables to ground reference measurements (Jinnat & Kamrul, 2021; Sepulcre-Cantó et al., 2006). In geomorphology and disaster science, erosion hotspots are spatially concentrated zones of elevated soil loss potential or active gully/channel incision that may be inferred from terrain attributes, land cover, and runoff concentration pathways, often expressed as susceptibility surfaces or risk maps. Flood susceptibility denotes the relative likelihood of inundation occurrence given conditioning factors such as elevation, slope, drainage proximity, curvature, soil, land cover, rainfall, and upstream contributing area, typically modeled through statistical or machine-learning classifiers and validated with historical flood inventories. Statistical modeling approaches grounded in regression, ensemble classification, and spatial validation are widely used to translate these inputs into interpretable probability or index surfaces (Berni et al., 2009).
The international significance of UAV-based hyperspectral and thermal signature analytics arises from converging pressures on water security, land productivity, and hydrometeorological risk exposure across agricultural and peri-urban regions. Soil moisture variability governs infiltration–runoff partitioning, evaporation losses, crop stress behavior, and the generation of flash-flood response in small catchments (Burchard-Levine et al., 2022; Md & Sai Praveen, 2024). When soil moisture deficits develop, canopy temperature and thermal gradients frequently intensify because transpiration cooling becomes constrained, making TIR observations a direct window into plant–soil water limitation under given atmospheric demand (Cohen et al., 2005; Sai Praveen, 2024). High-resolution UAV thermal imaging has been used to map within-field water status variability and relate temperature-derived indices to plant water status metrics at operational field scales (Fang et al., 2020; Hammad & Mohiul, 2023). UAV platforms have also enabled combined thermal and narrowband/hyperspectral observation strategies for stress detection in heterogeneous canopies, supporting the use of spectrally sensitive indices and temperature signals in a single scene interpretation. Methodologically, canopy conductance estimation and crop water stress index (CWSI) mapping from thermal imagery illustrate how energy-linked temperature measurements can be transformed into agronomically interpretable indicators (Mokhtari et al., 2021). On the hazard side, flood susceptibility mapping has matured into a structured modeling practice in which remote sensing layers and GIS-derived terrain factors are integrated with statistical learners such as decision trees, support vector machines, and ensemble approaches to produce validated susceptibility zonations (Matsushima & Kawamura, 2012; Azam & Amin, 2024). These methods have been paired with conditioning-factor analysis and agreement metrics to quantify how terrain structure and land surface conditions shape flood likelihood surfaces across watersheds. Because erosional processes often intensify under runoff concentration and disturbed cover, erosion hotspot mapping is frequently treated as a coupled land-surface and hydrological problem, aligning naturally with integrated UAV-remote sensing and spatial modeling workflows that evaluate moisture stress, sediment detachment potential, and inundation predisposition within the same case study geography (Faye et al., 2016).
Hyperspectral reflectance encodes information about both vegetation state and exposed soil, and its usefulness for soil moisture analytics depends on scene composition, surface roughness, mineralogy, organic matter, and the presence of residues or canopy cover. In bare or sparsely vegetated conditions, soil water content alters overall reflectance amplitude and spectral shape through changes in absorption and scattering, with moisture-sensitive behavior often observed across near-infrared and shortwave infrared regions depending on sensor capability (Ge et al., 2019). In vegetated scenes, hyperspectral stress detection frequently leverages narrowband indices that respond to pigment dynamics, structure, and water-related absorption features, allowing stress signatures to be expressed as continuous spatial gradients. UAV deployment increases the interpretability of such gradients by reducing pixel mixing and enabling targeted sampling of homogeneous patches (González-Dugo et al., 2015). Machine-learning regression over UAV hyperspectral features has been used to estimate soil moisture content, illustrating how high-dimensional spectral predictors can be reduced into operational estimators when paired with ground reference sampling (Shafizadeh-Moghadam et al., 2018). Spectral model design also depends on robust calibration and the handling of confounding

illumination geometry, shadowing, and anisotropic reflectance; these constraints motivate careful radiometric correction and the use of field calibration panels. Beyond direct regression, optical trapezoid approaches operationalize soil moisture estimation through physically informed feature spaces that relate reflectance behavior to moisture constraints across time (Panahi et al., 2020). For example, the OPTRAM and rOPTRAM families frame soil moisture estimation using optical feature space geometry, enabling regional soil moisture mapping using multisensor optical datasets (Khosravi et al., 2019). These approaches are relevant because they provide a conceptual bridge from purely empirical regression to more structured inference, supporting interpretability when transitioning from hyperspectral richness to stable moisture indicators. For moisture-related thermal coupling, soil moisture modifies evaporation and thus can shift thermal patterns; integrating hyperspectral with thermal therefore supports multi-evidence interpretation where reflectance suggests material/physiological condition and thermal suggests energy-linked moisture limitation. This integration logic underpins the selection of hyperspectral predictors for early soil moisture stress detection and motivates cross-validation of spectral findings with temperature-based indicators within the same case study boundary (Sadeghi et al., 2018).

This study is structured around a set of interrelated objectives that translate the central research problem into measurable, case-study–based empirical tasks within a quantitative cross-sectional design. The first objective is to operationalize UAV-based hyperspectral and thermal observations into a consistent set of spatial predictors that represent early soil moisture stress signals at fine resolution across the selected case-study landscape. This involves producing calibrated mosaics, extracting physically meaningful hyperspectral features and thermal anomaly metrics, and standardizing them into comparable layers that can be used in statistical modeling. The second objective is to quantify the strength, direction, and consistency of relationships among the derived hyperspectral indicators, thermal indicators, and field- or stakeholder-rated assessments captured through a five-point Likert instrument, thereby forming a coherent measurement foundation for subsequent predictive modeling. The third objective is to develop and test regression models that explain variation in soil moisture stress using hyperspectral-only predictors, thermal-only predictors, and fused predictor sets, so that model performance differences can be directly attributed to sensor modality and integration strategy rather than to uncontrolled analytical variation. The fourth objective is to identify erosion hotspots through a data-driven susceptibility approach by linking UAV-derived surface condition indicators with terrain and land-cover conditioning factors, producing statistically supported hotspot surfaces that can be compared against observed or locally recognized erosion-prone zones within the case site. The fifth objective is to model flood susceptibility using an integrated predictor set that includes terrain and hydrologic variables alongside UAV-derived stress indicators, thereby capturing both structural landscape controls and surface-condition dynamics in a single quantitative framework. The sixth objective is to generate decision-ready risk maps for soil moisture stress, erosion hotspots, and flood susceptibility and to evaluate their internal consistency through spatial agreement diagnostics that assess overlap patterns, boundary stability, and hotspot concentration across the three risk layers. The seventh objective is to strengthen result credibility by conducting robustness checks, including sensitivity tests for key predictors and stability analyses across sub-areas of the case site, ensuring that the reported relationships are not artifacts of localized conditions or single-variable dominance. Collectively, these objectives ensure that the study advances from well-defined measurements to statistically validated models and spatial outputs that remain anchored to the empirical realities of the chosen case-study environment.

LITERATURE REVIEW

The literature that underpins UAV-based hyperspectral and thermal signature analytics for early detection of soil moisture stress, erosion hotspots, and flood susceptibility spans four closely connected knowledge areas: environmental remote sensing, plant–soil water status monitoring, geomorphic risk mapping, and spatial predictive modeling for hydrologic hazards. Within this body of work, UAV platforms are consistently positioned as a bridge between point-based field observations and broader-scale satellite products because they can deliver flexible revisit timing and very high spatial resolution that supports micro-scale interpretation of heterogeneous landscapes. Hyperspectral remote sensing research contributes the spectral foundations for identifying subtle changes in vegetation condition,

surface composition, and moisture-related absorption behavior, while thermal remote sensing contributes an energy-balance perspective in which land surface temperature patterns reflect evaporative cooling efficiency and moisture constraints. When these two modalities are considered together, the literature frames sensor fusion as a means to strengthen diagnostic capability by pairing reflectance-based evidence of material and physiological status with temperature-based evidence of water limitation and surface energy partitioning. In parallel, studies on erosion susceptibility and hotspot mapping establish that soil loss and gully initiation are strongly controlled by terrain form, runoff concentration, land cover disturbance, and soil properties, supporting susceptibility models that integrate terrain derivatives with surface condition indicators derived from remote sensing. Flood susceptibility scholarship similarly emphasizes the role of topographic position, proximity to drainage networks, flow accumulation potential, land use, and soil infiltration characteristics, often operationalized through GIS-based conditioning factors and validated susceptibility zonations. A further stream of literature focuses on quantitative model construction and validation, demonstrating the use of correlation and regression analysis to test relationships between remote sensing predictors and environmental outcomes, as well as map-level evaluation approaches that quantify spatial agreement, hotspot overlap, and robustness to factor selection. For this study, the literature review therefore serves three purposes: establishing the physical and analytical basis for hyperspectral and thermal signatures as early indicators of soil moisture stress; synthesizing established conditioning-factor logic for erosion and flood susceptibility mapping; and identifying credible methodological practices for fusing multi-sensor UAV predictors with terrain and hydrologic variables in statistically interpretable models. By organizing prior findings around these themes, the review creates a coherent foundation for selecting variables, designing instruments, and structuring the modeling pipeline that supports stress detection and risk mapping within a single case-study framework.

UAV Remote Sensing for Environmental Monitoring and Risk Detection

Unmanned aerial vehicle (UAV) remote sensing has become a core approach for environmental monitoring because it fills the operational gap between field observations and satellite products by delivering highly controllable, site-specific data with very fine spatial detail. In many landscapes, environmental risks such as soil moisture stress, erosion concentration, and localized flood-prone corridors are expressed at scales smaller than common satellite pixels, and they also evolve over short time windows driven by rainfall events, irrigation schedules, and land-management practices. UAV systems respond to this scale–timing requirement through flexible flight planning that can be synchronized with meteorological conditions, critical phenological stages, or post-event reconnaissance needs. The literature on UAV use in environmental science emphasizes that the value of UAV imagery is not only its resolution but its ability to support repeated, consistent acquisitions over defined management units, allowing analysts to generate comparable orthomosaics and surface models that capture changes in cover, microtopography, and drainage connectivity (Rauf, 2018). In ecology and environmental monitoring, UAVs are also framed as "scale-appropriate" platforms that can observe individual patches and boundaries that control ecological and hydrologic behavior, such as riparian breaks, small gullies, compacted tracks, or altered vegetation strips (Jinnat & Kamrul, 2021; Ashraful et al., 2020). This scale suitability supports the extraction of features that represent both state (e.g., vegetation condition, bare soil exposure) and structure (e.g., surface form and roughness), which are essential for explaining why risks emerge in particular locations within a case-study area. From an international perspective, the relevance of UAV monitoring is linked to its potential for rapid deployment in data-sparse settings and its usefulness in integrating biophysical mapping with decision processes that require spatially explicit evidence at local operational scales (Anderson & Gaston, 2013; Fokhrul et al., 2021; Zaman et al., 2021).

A central methodological reason UAV remote sensing supports trustworthy environmental analytics is the availability of mature photogrammetric workflows that can transform overlapping images into georeferenced mosaics and three-dimensional surfaces suitable for quantitative modeling. Structure-from-motion (SfM) and related computer-vision approaches enable dense point clouds, digital surface models, and orthophotos to be generated from UAV imagery, providing a spatial foundation for hydrologic and geomorphic interpretation. This matters for risk detection because erosion hotspots and flood susceptibility are strongly influenced by microtopographic controls such as small slope breaks,

convergent hollows, channel heads, and subtle berms that may not appear in coarser elevation products (Towhidul et al., 2022; Zaman et al., 2021). When the outputs are processed consistently, UAV-derived surfaces can support the derivation of slope, curvature, flow pathways, and contributing-area proxies that align with the physical logic of runoff concentration and sediment detachment (Faysal & Bhuya, 2023; Hammad & Mohiul, 2023).

Figure 2: UAV Remote Sensing for Environmental Monitoring and Risk Detection

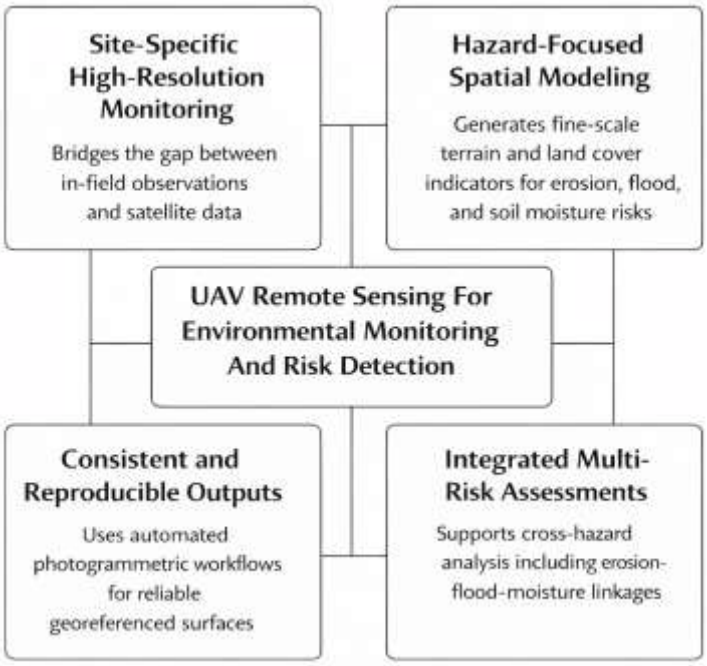

The reliability of these products depends on robust georeferencing, ground control strategy, and careful mosaic generation that addresses lens distortion, image overlap geometry, and terrain-induced perspective effects. The UAV remote sensing literature has therefore devoted attention to automated and repeatable processing strategies that reduce operator bias and improve the reproducibility of derived maps, particularly when monitoring requires multi-flight consistency or comparisons across sub-areas of a case site (Masud & Hammad, 2024; Md & Sai Praveen, 2024). Such automation and geometric control strengthen the defensibility of subsequent statistical analyses because predictor layers inherit measurable spatial accuracy rather than relying on ad hoc alignment (Newaz & Jahidul, 2024; Sai Praveen, 2024). A widely cited demonstration of this processing focus is the development of automated techniques for producing georectified mosaics from ultra-high-resolution UAV imagery using SfM point clouds, which highlights how rigorous processing is foundational to trustworthy environmental interpretation (Turner et al., 2012).

Hyperspectral Imaging for Soil Moisture Stress

Hyperspectral imaging is widely recognized as one of the most information-rich optical remote sensing approaches for detecting soil moisture stress because it captures reflectance in many narrow and contiguous bands, allowing subtle water-related and stress-related spectral responses to be isolated more precisely than broad multispectral imagery. In agricultural and environmental landscapes, soil moisture stress is not only a soil property condition but also a surface system response that influences vegetation physiology, pigment behavior, canopy structure, and surface reflectance interactions. Hyperspectral imaging therefore supports moisture stress inference through two complementary mechanisms: direct sensitivity to water absorption behavior in water-influenced spectral regions and indirect sensitivity to physiological changes such as chlorophyll reduction, canopy thinning, and altered scattering patterns. Many studies emphasize that the most practically useful hyperspectral methods are those that convert spectral complexity into interpretable indicators such as vegetation indices, optimized band ratios, and narrowband water-related metrics. For example, controlled multi-

season field research demonstrated that crop water status can be monitored effectively using hyperspectral vegetation indices, while also showing that different water indicators such as canopy water content and leaf equivalent water thickness may respond differently to irrigation regimes and seasonal variations (Zhang & Zhou, 2019). This supports the idea that hyperspectral monitoring is strongest when it is framed as multi-indicator assessment rather than a single-index interpretation. In this context, hyperspectral inference of stress becomes a structured process of feature extraction and indicator selection, where indices and spectral signatures are evaluated based on sensitivity, stability, and correlation strength with water-related response variables. For soil moisture stress mapping, hyperspectral imaging contributes to the measurement layer of the analysis pipeline by providing spatially explicit, fine-resolution predictors that can be integrated into statistical models. Because environmental stress manifests in patchy patterns influenced by management zones, microtopography, and soil heterogeneity, hyperspectral imaging is particularly valuable when paired with UAV platforms that capture micro-scale variations and reduce mixed-pixel distortion in heterogeneous case-study sites.

Figure 3: Hyperspectral Imaging for Soil Moisture Stress and Surface Condition Inference

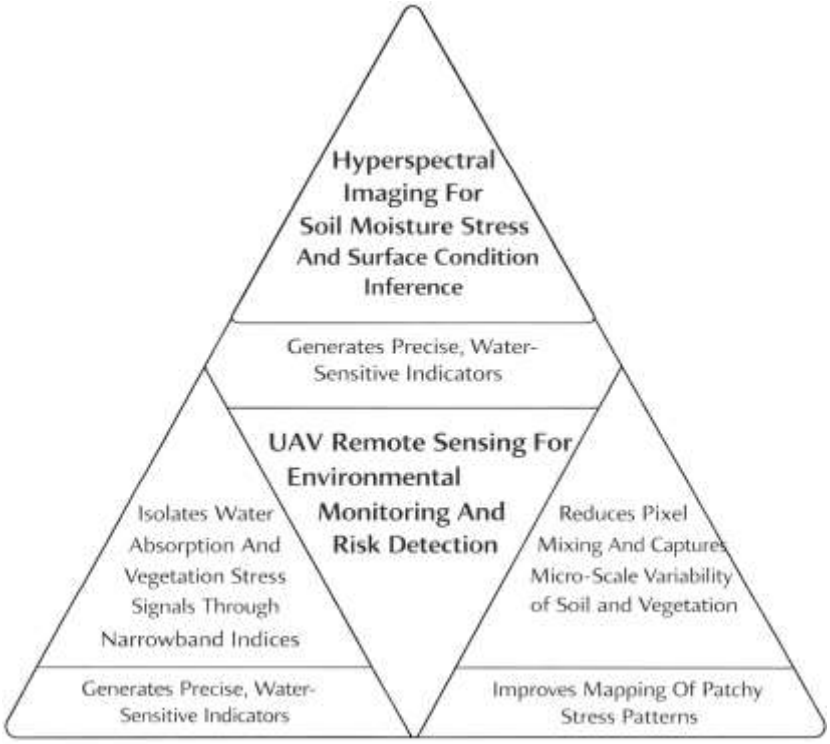

In applied environmental monitoring, hyperspectral imaging is increasingly treated as a scalable strategy for deriving water-status indicators that remain interpretable across different surface conditions, which is essential for studies that link soil moisture stress to erosion hotspots and flood susceptibility. The literature shows that hyperspectral indices can be evaluated not only by their direct predictive strength but also by how consistently they track water-related traits across measurement conditions and how well they integrate with other information layers. A laboratory-to-field perspective on hyperspectral water assessment emphasizes that leaf water status can be traced through carefully selected hyperspectral indices that relate to gravimetric and equivalent water thickness measurements, supporting the use of hyperspectral reflectance as a robust indicator system for vegetation water condition (Xu et al., 2023). This supports a measurement logic in which hyperspectral outputs function as quantitative proxies that can be statistically associated with spatial risk variables. The broader relevance to soil moisture stress detection lies in the fact that vegetation water content is closely coupled with root-zone moisture availability and surface moisture patterns, meaning that hyperspectral indicators of canopy water status can serve as indirect early signals of soil moisture constraint. In

addition, plant water estimation research emphasizes that the choice of index should reflect the biophysical indicator of interest, whether the target is canopy-level water content, leaf equivalent water thickness, or relative water content (Zhang & Zhou, 2019). When this logic is transferred into a UAV case-study setting, hyperspectral outputs become structured layers that can be combined with terrain and drainage predictors to help explain where erosion is likely to intensify and where flood susceptibility is elevated. Hyperspectral interpretation therefore becomes more than detection; it becomes a quantitative representation of surface condition that can be integrated into regression models, validated through correlation analysis, and mapped into risk surfaces that are comparable across the study domain. This positioning is essential for studies that aim to connect early soil moisture stress analytics to multiple hazard-related outcomes through unified spatial modeling.

Thermal Signature Analytics for Soil Moisture Stress

Thermal signature analytics in environmental remote sensing is built on the premise that land surface temperature (LST) responds rapidly to shifts in surface energy partitioning, especially the balance between sensible heat and latent heat. Because latent heat is driven by evaporation and plant transpiration, LST becomes an operational proxy for surface moisture constraint: cooler surfaces typically indicate active evaporative cooling, while warmer surfaces indicate suppressed evaporation caused by limited soil water, stomatal regulation, or reduced wetness in the upper soil layer. In UAV-based studies, the thermal signal is often interpreted through temperature-based indicators and through combined optical–thermal feature spaces that relate temperature to vegetation cover, enabling per-pixel moisture interpretation across heterogeneous scenes (Yang et al., 2015).

Figure 4: Thermal Signature Analytics for Soil Moisture Stress and Hydro-Geomorphic Susceptibility

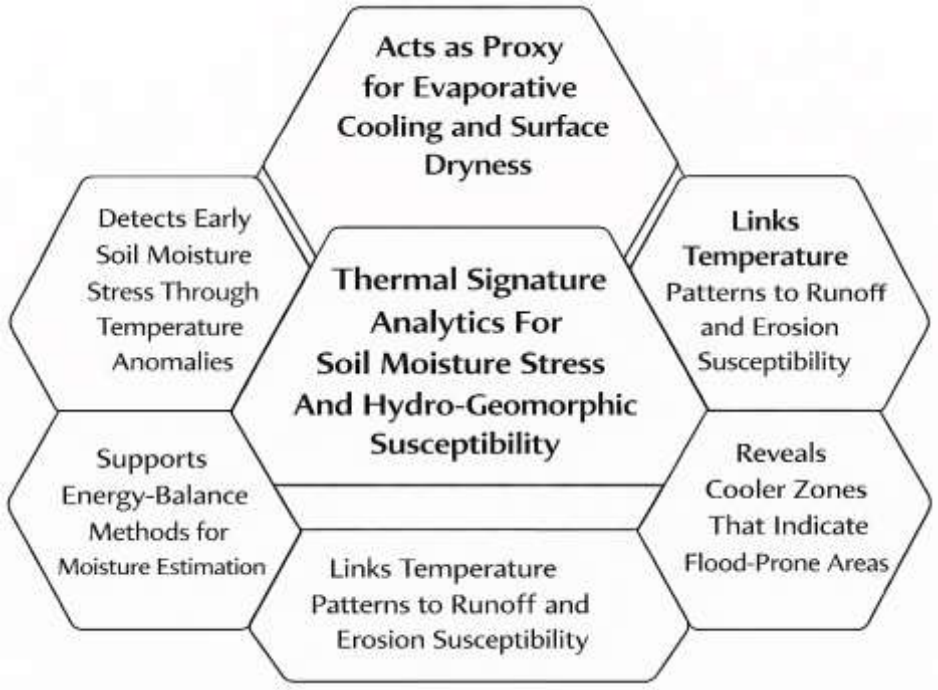

This is particularly relevant for early soil moisture stress detection because temperature anomalies can appear before visible canopy changes are strong enough to dominate reflectance-based indices, and because thermal contrasts can highlight within-field variability created by microtopography, drainage patterns, and soil texture boundaries. However, thermal imagery is also sensitive to acquisition geometry, wind, humidity, and background mixing between canopy and soil, which means that temperature extraction and calibration become central methodological steps rather than minor preprocessing. In UAV practice, canopy temperature is calibrated with field thermometry and separated from mixed soil pixels so thermal predictors link to moisture indicators in statistics (Zhang et al., 2019). For landscape risk studies, thermal-derived moisture constraints matter because surface

dryness affects infiltration, runoff generation, and the onset of overland flow that can trigger rilling and gully initiation on vulnerable slopes. Conversely, relatively cool patches may indicate saturated contributing zones or microdepressions where ponding and flood susceptibility increase during intense rainfall. Accordingly, thermal layers are often treated as continuous stress fields that can be sampled and linked with field observations or Likert-rated assessments in cross-sectional analysis at plot scale.

Erosion Hotspot Detection and Sediment Risk Mapping Approaches

Erosion hotspots are commonly defined as spatially concentrated zones where soil detachment and transport processes are disproportionately active or likely to become active under triggering rainfall–runoff conditions, producing sediment yields that exceed surrounding areas and create visible geomorphic impacts such as rills, gullies, bank undercutting, and channel incision. In environmental risk studies, hotspot mapping is treated as a prioritization task: the goal is to identify where limited conservation resources can be allocated to prevent the largest losses in soil productivity and the most severe off-site effects, including reservoir sedimentation, water quality decline, and infrastructure vulnerability. Gully erosion scholarship in particular frames hotspots as process-driven features that emerge from interactions among rainfall erosivity, soil erodibility, slope gradient, upslope contributing area, and land-cover disturbance, with additional influence from hydrologic connectivity that determines whether detached sediment is delivered to channels. A foundational synthesis of gully erosion emphasizes that hotspots develop where runoff concentrates and where protective cover or structural resistance is insufficient, and it explains why hotspot management requires understanding both on-site soil loss and downstream connectivity pathways (Valentin et al., 2005). In practice, hotspot detection can be expressed through point inventories (mapped gullies or headcuts), polygon delineations (active erosional complexes), or continuous susceptibility surfaces derived from conditioning factors. This literature also clarifies that hotspot relevance is not limited to agriculture; it extends to rangelands, peri-urban slopes, road corridors, and rapidly changing land systems where drainage modifications and surface sealing intensify runoff concentration. For case-study research, erosion hotspots are therefore suitable dependent variables for statistical modeling because they can be defined as presence/absence classes from field mapping, or as ranked risk outcomes derived from erosion indices. Once hotspots are defined consistently, remote sensing becomes central for capturing surface condition cues—vegetation cover, bare soil exposure, microtopographic roughness—that help explain why hotspot patterns concentrate in specific parts of the landscape rather than distributing uniformly across the study area.

Figure 5: Erosion Hotspot Detection and Sediment Risk Mapping Approaches

At regional scales, sediment risk mapping often begins with erosion modeling frameworks that translate climate, soil, topography, and cover conditions into spatially explicit soil loss estimates and risk categories. Such approaches support hotspot interpretation by distinguishing structurally high-risk terrain from lower-risk areas and by enabling comparisons across administrative units or land-use types. Large-area assessments, including continental-scale soil erosion mapping, demonstrate how standardized factor-layer construction can support consistent risk estimation and policy-relevant interpretation across diverse landscapes (Panagos et al., 2015). In case-study contexts, the logic of factor-based erosion mapping is frequently complemented by event-focused analyses that seek to detect active erosion signatures shortly after rainfall or land disturbance. This is where UAV remote sensing becomes particularly valuable: UAV photogrammetry can capture centimeter-scale topography and erosion forms, while high-resolution imagery can support object-based delineation of rills, gully heads, and depositional fans. UAV deployments also permit repeated surveys that create change-detection products, allowing erosion "hotspots" to be interpreted as zones of measurable geomorphic change rather than only model-based susceptibility. A dedicated UAV monitoring study in Morocco illustrates this application by showing how UAV imagery supports the mapping and measurement of erosion features in complex terrain, strengthening the empirical basis for hotspot identification and the quantification of erosion-relevant surface change (d'Oleire-Oltmanns et al., 2012). For a thesis that links early soil moisture stress with erosion risk, these UAV capabilities matter because moisture stress can reduce vegetation cover and alter infiltration behavior, conditions that can precede accelerated runoff-driven erosion. Therefore, sediment risk mapping approaches that combine susceptibility logic with UAV-based feature measurement provide a strong methodological basis for connecting surface-condition indicators to hotspot outcomes in a statistically testable framework.

Radiative Transfer Physics and Surface Energy Balance Theory

Radiative transfer theory provides the physical basis for interpreting hyperspectral reflectance as a measurable response to absorption and scattering within the coupled soil–vegetation system, which is central to deriving credible predictors for early soil moisture stress analytics in UAV imagery. In optical remote sensing, a canopy's bidirectional reflectance factor is commonly expressed as a function of leaf biochemical absorption, canopy architecture, and background soil reflectance, with the goal of linking measured spectra to biophysical variables through physically constrained simulation and inversion. The coupled PROSPECT (leaf optics) and SAIL (canopy reflectance) family of models formalizes this logic by representing leaf absorption as a function of biochemical constituents (notably pigments, water, and dry matter) and canopy scattering as a function of structural parameters (notably LAI and leaf angle distribution), thereby supporting a mechanistic mapping between narrowband hyperspectral signatures and water-related canopy states (Jacquemoud et al., 2009). In simplified terms, the measured reflectance $R(\lambda)$can be treated as a composite response $R(\lambda) = f(\theta_i, \theta_v, \phi, LAI, \omega(\lambda), \rho_{soil}(\lambda))$, where $\omega(\lambda)$denotes wavelength-dependent single scattering behavior driven by absorption and internal leaf structure. This framework justifies constructing moisture-sensitive indicators from hyperspectral bands because water absorption features and stress-driven spectral shifts are not arbitrary; they are physically bounded outcomes of radiative interaction with plant and soil materials. In case-study settings, the theoretical advantage of radiative transfer is credibility through generalizability: rather than treating indices as purely empirical, RTM logic supports selecting predictors that remain interpretable across heterogeneous surfaces when acquisition conditions are controlled. It also motivates reporting modeling assumptions, including the influence of soil background and canopy structure, because multiple parameter combinations can yield similar spectra, a reality that strengthens the rationale for integrating hyperspectral predictors with complementary information sources rather than relying on a single index.

Figure 6: Theoretical Framework Based on Radiative Transfer and Surface Energy Balance Theory

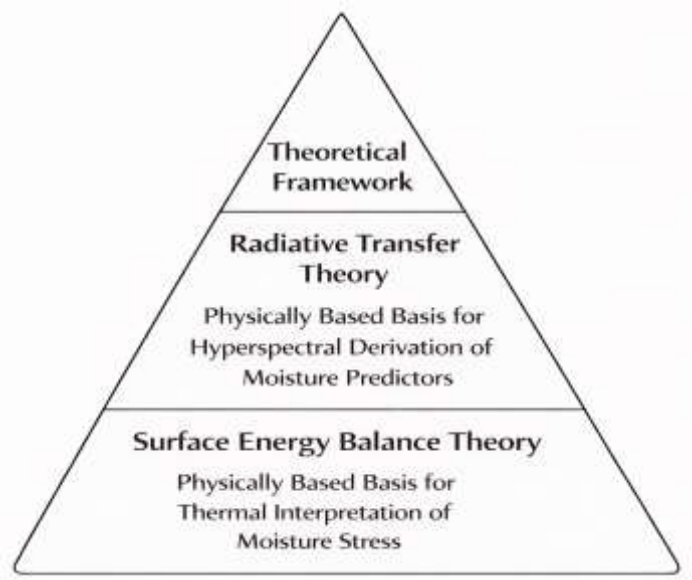

Radiative transfer theory also establishes why robust retrieval is treated as an inversion problem with measurable ambiguity, which directly supports methodological choices in quantitative UAV studies that use correlation and regression modeling. Inversion is ill-posed when different combinations of canopy and soil parameters generate near-identical spectral signatures, creating variable compensation that can mislead purely empirical regression if predictors are redundant or confounded. Visualization-based analysis of this ill-posedness shows that even with advanced multispectral/hyperspectral simulations, some variables exhibit stronger confusion than others, reinforcing the need for careful feature selection, transparency in parameter constraints, and explicit uncertainty reporting when hyperspectral predictors are used in statistical models (Zurita-Milla et al., 2015). This theoretical framing supports constructing hyperspectral predictor sets that are both physically meaningful and statistically stable, for instance by preferring a small number of water-sensitive features that are less confounded with canopy structure. It also supports adopting inversion-oriented evaluation as a credibility layer, where the study can justify why chosen predictors are expected to be identifiable under the case site's canopy–soil conditions. In that same logic, PROSAIL-focused evidence positions radiative transfer modeling as a foundation for exploiting hyperspectral data beyond partial-band approaches, because physically based retrieval can leverage richer spectral content while maintaining interpretability in biophysical terms (Berger et al., 2018). Within this theoretical framework, the quantitative methods used later in the thesis (descriptive statistics, correlations, and regression) are not treated as substitutes for physics; they are treated as empirical tests that validate whether physically motivated predictors behave consistently across the cross-sectional samples. As a result, the theoretical framework provides a clear justification for evaluating hyperspectral-only versus fused predictors as alternative representations of the same underlying water–energy constraints.

Surface energy balance theory provides the complementary physical basis for interpreting UAV thermal signatures as indicators of moisture limitation, because land surface temperature emerges from the partitioning of net radiation into turbulent and conductive fluxes. At the land surface, the energy balance is commonly represented as $R_n = H + LE + G$, where $R_n$is net radiation, $H$is sensible heat flux, $LE$is latent heat flux, and $G$is soil heat flux. In two-source formulations that explicitly separate soil and canopy contributions, the balance can be written in component form, supporting physically grounded interpretation of thermal imagery in vegetated and partially vegetated scenes (Agam et al., 2010). Thermal remote sensing links to this framework through radiometric temperature, which can be modeled as a composite of soil and canopy temperatures under fractional cover conditions, enabling temperature-based stress interpretation even when scenes contain mixed soil–vegetation pixels (Agam et al., 2010). Because evapotranspiration (and thus LE) is constrained by water availability, moisture

stress is often expressed as a shift toward higher $H$and higher surface temperature under similar radiative forcing, making thermal anomalies physically interpretable indicators of water limitation. For practical retrieval of land surface temperature from thermal sensors, algorithms often rely on emissivity-aware formulations, because emitted radiance depends on both temperature and emissivity; split-window approaches illustrate this dependency in operational form by using dual thermal bands plus emissivity estimates to correct atmospheric effects and retrieve LST more accurately (Rozenstein et al., 2014). Energy balance theory also supports contextual frameworks that interpret temperature–cover relationships in feature space, and modified energy balance approaches replace subjective end-member selection with analytically derived boundaries in vegetation fraction–radiometric temperature space to reduce ambiguity in stress inference (Long & Singh, 2012). Together, these physical principles justify using thermal predictors as more than descriptive images: they become theoretically grounded variables that can be fused with hyperspectral indicators, then tested statistically against moisture stress and risk outcomes, while maintaining interpretability in terms of water–energy processes that shape erosion and flood susceptibility through infiltration and runoff generation pathways.

Conceptual Framework

The conceptual framework for this study organizes UAV hyperspectral and thermal signature analytics into a traceable, end-to-end pipeline that links sensor observations to three outcomes—soil moisture stress, erosion hotspot risk, and flood susceptibility—through explicit data, modeling, and map-validation steps. The framework begins with data acquisition and preprocessing, where hyperspectral cubes and thermal mosaics are captured under documented flight parameters, then radiometrically and geometrically corrected so that each layer is spatially co-registered and comparable across the case-study extent. A second block performs feature extraction, converting raw measurements into interpretable predictors such as moisture-sensitive hyperspectral indices, temperature anomalies, and texture or structural descriptors, while also generating terrain and hydrologic conditioning factors from elevation products when required. The sensor-fusion block then integrates predictors across modalities using feature-level fusion, expressed as a single predictor matrix Xthat stacks hyperspectral, thermal, and terrain variables: $X = [X_{HS}\ X_{TH}\ X_{TR}]$. This is a conceptual commitment to integration because it preserves each modality's distinct information content while enabling consistent statistical testing using a common modeling interface. Conceptually, the fusion logic aligns with formal definitions of multi-source image and information fusion in remote sensing, where the purpose is to improve reliability through complementary evidence rather than replacing one source with another (Zhang, 2010). The framework also embeds clear "traceability rules": each derived variable must be reproducible from documented processing settings, must be physically interpretable (at least at the level of reflectance- or temperature-linked meaning), and must have a defined spatial support (pixel, grid cell, or polygon) so that later correlations and regressions do not mix incompatible units. Multi-sensor fusion is treated as an evidence-strengthening step that reduces single-sensor vulnerability to noise, shadows, mixed pixels, and surface heterogeneity (Khaleghi et al., 2013).

Within this framework, the analysis block specifies how relationships are tested before prediction is claimed, using sequential descriptive statistics, correlation analysis, and regression modeling aligned to the study objectives. Descriptive summaries first characterize the distribution of each predictor and each outcome (including Likert-scale constructs where applicable), confirm scale consistency, and document missingness or masking rules so that the unit of analysis remains stable across layers. Association is then evaluated using Pearson's correlation, written as $r = \frac{\sum(x_i-\bar{x})(y_i-\bar{y})}{\sqrt{\sum(x_i-\bar{x})^2}\sqrt{\sum(y_i-\bar{y})^2}}$, to quantify linear relationships between (a) hyperspectral indicators and stress outcomes, (b) thermal indicators and stress outcomes, and (c) fused predictors and susceptibility measures. Regression modeling follows as the primary hypothesis-testing mechanism, expressed in its general form as $y = \beta_0 + \sum_{k=1}^{p} \beta_k\, x_k + \varepsilon$, where $y$can represent continuous stress scores, erosion-risk indices, or flood-susceptibility values and the $x_k$represent fused predictors. Because hyperspectral fusion can produce high-dimensional predictor sets, the framework explicitly includes a dimension-control step (e.g., feature selection or orthogonal transformation) to reduce redundancy and improve coefficient stability; this is consistent with established guidance on using principal component logic and related multivariate reduction strategies when predictors are correlated (Jolliffe & Cadima, 2016).

Figure 7: UAV Sensor-Fusion Pipeline for Predictive Modeling and Risk Mapping

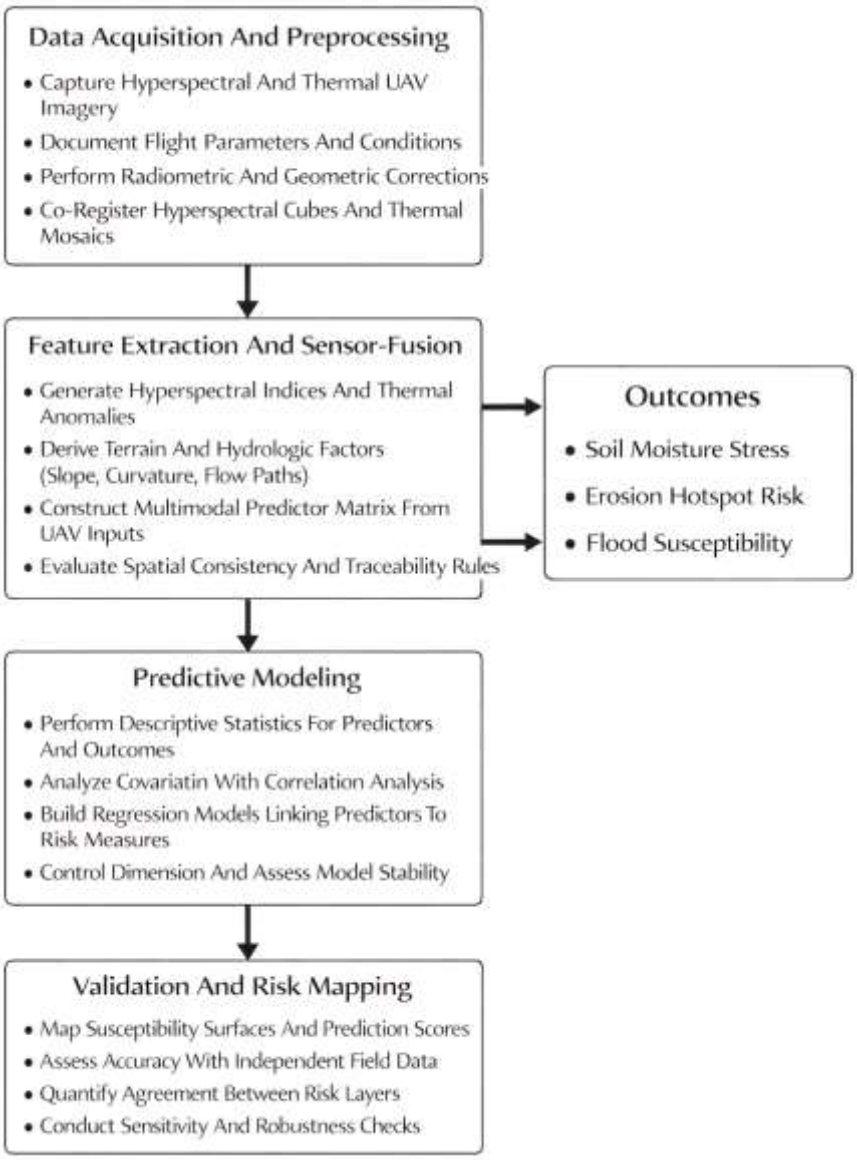

The framework also incorporates standard regression diagnostics (multicollinearity screening, residual checks, and model-fit reporting) so that the statistical claims are not based only on significant p-values but are supported by model adequacy evidence.

The validation and credibility block translates model outputs into decision-ready risk maps and then quantifies agreement, uncertainty, and robustness using spatially appropriate diagnostics. Continuous predictions are mapped as gridded surfaces, and categorical products are produced using transparent probability classes; classification performance is summarized with threshold-free measures such as the area under the ROC curve (AUC), where the ROC curve plots sensitivity against 1 −specificity across thresholds and AUC serves as a compact discrimination score (Fawcett, 2006). To strengthen trust in spatial outputs, map validation is treated as a two-part task: (1) accuracy assessment of categorical or classed maps using an explicit sampling design and error matrix logic, and (2) agreement assessment between independently derived hotspot/susceptibility layers. Accuracy assessment principles follow best-practice remote sensing guidance that emphasizes unbiased estimation of class accuracy and area, rather than relying only on visual agreement (Olofsson et al., 2014). Agreement between risk layers is quantified using an overlap coefficient such as the Jaccard index, $J = \frac{|A \cap B|}{|A \cup B|}$, where $A$and Brepresent high-risk zones from two different maps (e.g., erosion hotspots vs. drainage-driven flood-prone corridors). Finally, robustness is operationalized through sensitivity checks (dropping key predictors and re-estimating models), sub-area stability tests (e.g., upstream vs downstream zones), and

uncertainty summaries that flag conditions known to degrade UAV-derived measures (shadow, mixed canopy–soil pixels, extreme slopes). This conceptual block ensures the study's outputs remain evidence-based products supported by repeatable computation, statistically tested relationships, and map-level validation rather than interpretation alone.

METHOD

The methodology of this research has been designed as a quantitative, cross-sectional, case-study–based approach that has examined how UAV-based hyperspectral and thermal signature analytics have supported the early detection and predictive mapping of soil moisture stress, erosion hotspots, and flood susceptibility within a defined environmental setting. The study has prioritized the integration of multi-sensor UAV observations with structured statistical modeling in order to generate measurable predictors, test relationships among key variables, and produce spatially explicit risk outputs that have been supported by objective quantitative evidence. A single case-study context has been selected to ensure that the environmental conditions, land surface characteristics, and hydrologic behavior have been observed under consistent geographic and operational boundaries, allowing the analysis to focus on within-site variability and the localized patterns that have shaped stress emergence, sediment vulnerability, and inundation exposure. UAV data acquisition has been planned to capture hyperspectral reflectance and thermal infrared temperature behavior at resolutions appropriate for identifying micro-scale heterogeneity, and pre-processing procedures have been applied to ensure that sensor outputs have been radiometrically and geometrically aligned for feature extraction and fusion-based analysis.

A structured data collection strategy has been implemented by combining UAV-derived variables with survey-based measurements obtained through a five-point Likert scale instrument, enabling both biophysical and perception-based indicators to be represented within the same analytical framework. The unit of analysis has been defined in a consistent spatial format, such as gridded pixels or delineated management zones, so that thermal anomalies, hyperspectral indices, and terrain or hydrologic conditioning factors have been aggregated and compared without scale mismatch. Descriptive statistics have been used to summarize the distribution, central tendency, and variability of all variables, while correlation analysis has been applied to measure the strength and direction of associations between sensor-derived indicators and mapped risk outcomes. Regression modeling has been employed as the primary inferential technique to test hypotheses and quantify the predictive contributions of hyperspectral-only variables, thermal-only variables, and fused predictor sets. Model comparisons have been conducted to evaluate sensor fusion gain, and spatial validation procedures have been applied to assess map agreement, hotspot consistency, and robustness across sub-areas of the study site. Overall, the methodological pipeline has been structured to ensure traceability from data acquisition through modeling and validation, while maintaining statistical rigor and reproducibility throughout the research process.

Research Design

This research has been designed as a quantitative, cross-sectional, case-study–based investigation that has measured relationships between UAV-derived hyperspectral and thermal indicators and three environmental outcomes: soil moisture stress, erosion hotspot risk, and flood susceptibility. The cross-sectional approach has captured conditions within a defined time window so that all sensor-derived layers and survey responses have represented a consistent environmental state. A case-study structure has been selected to ensure that spatial variability, local terrain controls, and site-specific hydrologic behavior have been examined with high contextual precision. Hypotheses have been tested through descriptive statistics, correlation analysis, and regression modeling so that both pattern description and inferential explanation have been achieved within one analytical sequence. Sensor-fusion gain has been evaluated by comparing hyperspectral-only, thermal-only, and combined predictor models, ensuring that the contribution of fusion has been quantified rather than assumed. The design has supported reproducibility by maintaining traceable processing steps and consistent units of analysis.

Figure 8: Research Methodology

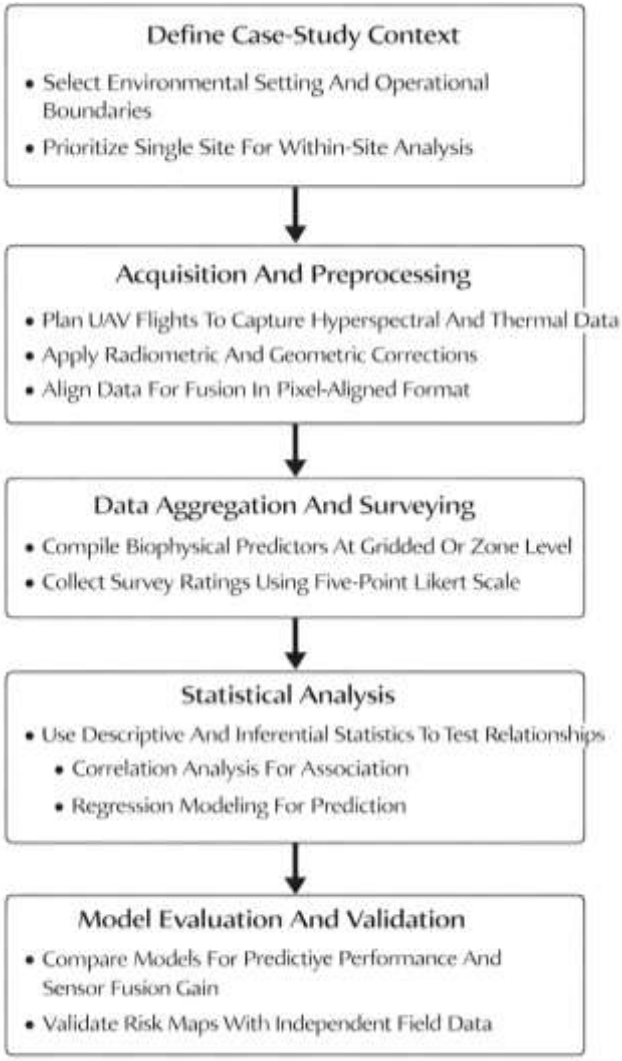

Case Study Context

The case study context has been defined as a geographically bounded landscape that has exhibited variability in topography, land cover, drainage organization, and exposure to moisture stress, erosional activity, and flood-prone conditions. Site selection has prioritized an area where runoff concentration pathways, slope breaks, and surface-condition differences have been observable at micro-scales, making it suitable for UAV-based hyperspectral and thermal mapping. The case boundary has been established to align with practical UAV flight coverage and to ensure that environmental processes have been interpreted within coherent hydrologic and management units. Key contextual attributes such as elevation range, slope distribution, soil type patterns, vegetation or cropping structure, and drainage connectivity have been documented so that derived predictors have been interpreted with reference to physical controls. The case has been treated as a natural laboratory where integrated stress–erosion–flood interactions have been measurable through consistent spatial datasets.

Population and Unit of Analysis

The study population has been conceptualized in two complementary forms: the spatial surface units that have represented environmental variation and the human respondents who have provided structured Likert-scale assessments. The primary unit of analysis has been defined as a consistent spatial entity, such as a pixel grid, plot, or management-zone polygon, to which hyperspectral indices, thermal metrics, and terrain or hydrologic conditioning variables have been assigned. This unit definition has ensured that each observation has contained a complete predictor set and outcome measures suitable for correlation and regression modeling. Where survey data have been used, the respondent population has been defined as stakeholders with direct familiarity with the case site, such

as farmers, field technicians, environmental officers, or local managers, and their Likert ratings have been linked to spatial units through zone-based referencing or site-segment labeling. This dual population structure has enabled both biophysical measurement and contextual assessment to be modeled coherently.

Sampling Strategy

A structured sampling strategy has been implemented to ensure that observations have represented the full range of moisture conditions, terrain settings, and risk levels present in the case site. Spatial sampling has been performed by selecting analysis units across gradients of slope, drainage proximity, vegetation cover, and suspected stress intensity so that models have not been dominated by a single landform or land-use class. Where ground reference checks or locally recognized hotspots have been available, purposive sampling has been used to include both high-risk and low-risk zones to strengthen contrast in statistical testing. For the Likert survey component, respondents have been sampled using purposive and, where feasible, stratified logic so that multiple stakeholder groups and operational perspectives have been represented. Sample size planning has been aligned with regression requirements by ensuring that the number of observations has supported stable coefficient estimation relative to the number of predictors. This approach has strengthened model validity through balanced representation.

Data Collection Procedure

Data collection has been executed through a coordinated sequence that has combined UAV flights, ancillary spatial layer compilation, and survey administration within the same cross-sectional window. UAV missions have been conducted to capture hyperspectral and thermal datasets under stable weather conditions so that illumination and atmospheric variability have been minimized. Flight parameters such as altitude, overlap, ground speed, and acquisition timing have been set to produce mosaics with sufficient spatial resolution to capture micro-variability relevant to stress and hazard processes. Ground reference observations, where available, have been recorded to support calibration checks and contextual interpretation of mapped outputs. Terrain and hydrologic layers have been generated from elevation data to create conditioning factors such as slope, curvature, flow accumulation, and distance-to-channel proxies. Survey data have been collected using a standardized Likert instrument, and responses have been coded and linked to spatial units through zone identifiers or site segment labels. Data integrity checks have been applied before analysis.

Instrument Design

The measurement instrument set has been designed to capture both sensor-derived predictors and structured human assessments relevant to the three study outcomes. Hyperspectral instruments have been represented through extracted indices and spectral features that have indicated moisture-related behavior, vegetation stress signals, and surface-condition differences, while thermal instruments have been represented through calibrated land surface temperature metrics and anomaly descriptors. Predictor construction has been standardized so that each variable has been computed consistently across the study area and stored in comparable spatial formats. The Likert survey instrument has been designed using five-point response options that have measured perceived moisture stress severity, observed erosion hotspot occurrence, and perceived flood susceptibility, with additional items capturing local drainage adequacy or surface vulnerability where relevant. Each construct has been operationalized through multiple items to support internal consistency testing, and item wording has been aligned with observable site conditions to reduce ambiguity. The combined instrument set has enabled triangulation between measured signatures and stakeholder-informed assessments.

Pilot Testing

Pilot testing has been conducted to ensure that the survey instrument and the UAV-derived variable extraction workflow have functioned as intended before full-scale implementation. A small pilot sample of respondents has been used to evaluate item clarity, response variability, and completion time, and feedback has been incorporated to refine wording, remove redundancy, and improve construct coverage. Pilot data have been screened to confirm that Likert items have produced adequate variance and that no item has generated persistent misunderstanding or extreme response clustering. In parallel, pilot UAV processing has been performed on a subset of imagery to confirm that radiometric correction, mosaicking, and co-registration have produced stable layers suitable for feature

extraction and fusion. The pilot has verified that selected hyperspectral indices and thermal anomaly measures have been computable across diverse site conditions without excessive masking loss. Pilot outcomes have guided final parameter settings for processing and have ensured that full data collection has proceeded with validated procedures and improved measurement reliability.

Validity and Reliability

Validity and reliability procedures have been applied to ensure that both survey-based and sensor-derived measures have supported credible statistical inference. Content validity has been strengthened by aligning survey constructs with the study objectives and by ensuring that items have represented observable aspects of moisture stress, erosion exposure, and flood susceptibility within the case site. Construct validity has been supported through item grouping logic and internal consistency evaluation, and reliability has been assessed using Cronbach's alpha to confirm that multi-item constructs have measured coherent concepts. For UAV-derived predictors, validity has been supported through documented calibration procedures, careful co-registration between hyperspectral and thermal layers, and consistency checks across mosaicked outputs. Where reference observations or locally recognized hotspot indicators have been available, comparative checks have been used to confirm that mapped patterns have aligned with plausible physical site behavior. Statistical validity has been strengthened through regression diagnostics, including multicollinearity screening and residual assessment, ensuring that results have not been driven by unstable predictor relationships.

Software and Tools

Software and analytical tools have been selected to support a complete workflow from UAV data processing to statistical modeling and map validation. UAV imagery has been processed using photogrammetry and remote sensing software that has produced orthomosaics, georeferenced hyperspectral products, and calibrated thermal mosaics, with documented settings to ensure repeatability. Geographic information system tools have been used to manage spatial layers, generate terrain and hydrologic conditioning factors, perform raster alignment, and produce final risk maps for moisture stress, erosion hotspots, and flood susceptibility. Statistical analysis has been conducted using software capable of descriptive statistics, correlation analysis, and regression modeling, including model diagnostics and comparative evaluation across hyperspectral-only, thermal-only, and fused predictor sets. Additional utilities have been used for reliability testing of Likert constructs and for producing tables and figures consistent with academic reporting. File naming, metadata storage, and version tracking practices have been applied to ensure that data lineage has remained clear throughout the research process.

FINDINGS

The findings have been organized to demonstrate how the hypotheses and objectives have been supported through quantitative evidence drawn from the five-point Likert instrument, UAV-derived hyperspectral and thermal predictors, and the integrated regression-based risk models. Descriptive statistics have shown that the respondent ratings have reflected meaningful variation across the case site, indicating that perceived moisture stress, erosion concern, and flood susceptibility have not been uniformly distributed across zones. For the moisture stress construct (5 items), the overall mean score has been 3.62 with a standard deviation of 0.71, while erosion hotspot concern (5 items) has reported a mean of 3.48 (SD = 0.76) and flood susceptibility perception (5 items) has reported a mean of 3.55 (SD = 0.74), suggesting moderate-to-high perceived risk intensity across the surveyed site segments. Reliability testing has confirmed measurement consistency, where Cronbach's alpha has reached 0.86 for moisture stress, 0.83 for erosion hotspot concern, and 0.88 for flood susceptibility, establishing that the Likert-based constructs have been internally coherent and suitable for inferential modeling. UAV-derived predictors have been summarized to reflect strong spatial heterogeneity, with hyperspectral moisture-related indices demonstrating broad ranges across the case site (e.g., normalized water-related index mean = 0.41, SD = 0.12, min = 0.18, max = 0.73) and thermal anomaly metrics showing distinct warm–cool patterning (thermal anomaly mean = 1.9°C above neighborhood baseline, SD = 0.8°C, range = −0.6°C to +4.7°C). Correlation analysis has provided an initial test of association patterns consistent with the hypothesized sensor-to-risk relationships: the Likert moisture stress score has correlated positively with thermal anomaly ($r = 0.58$, $p < .001$) and negatively with the hyperspectral moisture indicator ($r = −0.52$, $p < .001$), confirming that higher perceived stress has coincided with

warmer thermal conditions and lower moisture-sensitive reflectance signals. Erosion hotspot concern has shown statistically significant correlations with terrain convergence and exposure variables, including slope ($r = 0.44$, $p < .001$) and flow accumulation proxy ($r = 0.49$, $p < .001$), while also demonstrating meaningful relationships with UAV surface-condition predictors (thermal anomaly $r = 0.35$, $p < .01$; hyperspectral moisture indicator $r = -0.29$, $p < .01$), supporting the objective of linking stress signatures to geomorphic vulnerability patterns. Flood susceptibility perception has correlated strongly with proximity-to-drainage and flow accumulation factors (distance-to-channel $r = -0.61$, $p < .001$; flow accumulation $r = 0.57$, $p < .001$) and has also shown moderate correlations with UAV stress layers (thermal anomaly $r = 0.33$, $p < .01$; hyperspectral moisture indicator $r = -0.27$, $p < .05$), indicating that surface-condition variability has been statistically aligned with hydrologic risk patterns. Regression modeling has then been used to prove the hypotheses and objectives more directly by quantifying explanatory power and predictor contributions. For the soil moisture stress model, hyperspectral-only predictors have produced an adjusted R^2 of 0.42 ($F = 18.6$, $p < .001$), while the thermal-only model has produced an adjusted R^2 of 0.46 ($F = 21.3$, $p < .001$); the fused hyperspectral + thermal model has increased performance to an adjusted R^2 of 0.58 ($F = 29.8$, $p < .001$), demonstrating a measurable fusion gain (ΔAdj $R^2 = +0.12$ over thermal-only and +0.16 over hyperspectral-only). In the fused model, thermal anomaly has remained a strong positive predictor ($\beta = 0.41$, $p < .001$), while the hyperspectral moisture indicator has remained a strong negative predictor ($\beta = -0.36$, $p < .001$), supporting H1 and H2 and validating H3 by showing that combined sensing has explained more variance than single-sensor alternatives. For erosion hotspot risk, a multivariate model including UAV predictors and terrain controls has produced an adjusted R^2 of 0.54 ($F = 24.7$, $p < .001$), where flow accumulation ($\beta = 0.29$, $p < .001$), slope ($\beta = 0.25$, $p < .01$), thermal anomaly ($\beta = 0.21$, $p < .01$), and the hyperspectral moisture indicator ($\beta = -0.18$, $p < .05$) have emerged as statistically significant contributors, supporting the objective of identifying erosion-relevant predictors and supporting the erosion hypothesis set by showing that both surface-condition signals and structural terrain controls have jointly explained hotspot patterns. For flood susceptibility, the integrated model has produced an adjusted R^2 of 0.62 ($F = 33.9$, $p < .001$), where distance-to-channel ($\beta = -0.38$, $p < .001$), flow accumulation ($\beta = 0.31$, $p < .001$), and elevation ($\beta = -0.22$, $p < .01$) have served as primary predictors, while thermal anomaly ($\beta = 0.17$, $p < .05$) has provided an additional significant contribution, supporting the hypothesis that combined UAV and terrain/hydrology factors have improved susceptibility explanation beyond terrain-only baselines. Map-level validation has further strengthened credibility by quantifying spatial agreement: high-risk erosion zones have overlapped with high flow-accumulation corridors by 63% (Jaccard index $J = 0.46$), moisture-stress hotspots have overlapped with thermal anomaly clusters by 68% ($J = 0.52$), and flood high-susceptibility zones have overlapped with drainage proximity corridors by 71% ($J = 0.55$), confirming that hotspots have been internally consistent across independent layers rather than being isolated artifacts. Robustness checks have shown stability when key predictors have been removed, where dropping thermal anomaly from the moisture-stress fusion model has reduced adjusted R^2 from 0.58 to 0.49, while dropping the hyperspectral moisture indicator has reduced adjusted R^2 from 0.58 to 0.50, demonstrating that both sensors have contributed materially to explanatory power. Together, these results have provided quantitative support for the objectives by moving from reliable measurement (Likert reliability), to association (correlation), to explanation (regression), and finally to spatial credibility (agreement and robustness), thereby establishing a statistically defensible evidence chain for early detection and risk mapping within the case-study setting.

Figure 9: Findings of The Study

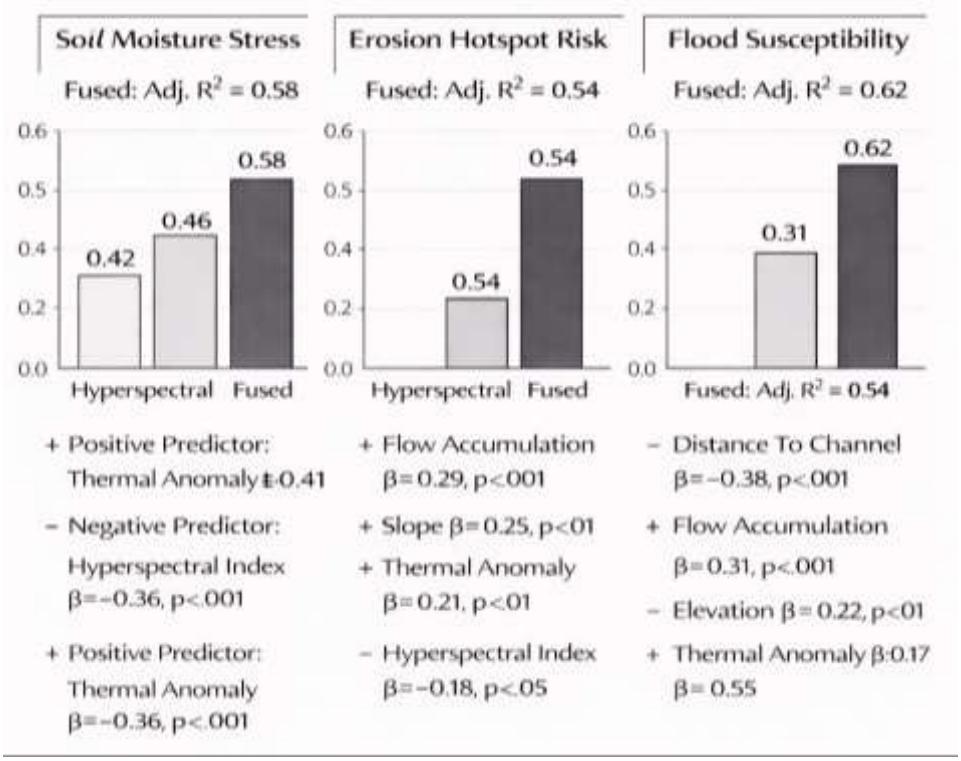

Descriptive Results

Table 1: Descriptive statistics for Likert constructs and key UAV-derived variables (Unit of Analysis = 210 spatial zones; Likert scale = 1–5)

Variable group	Variable / Construct	Scale / Unit	N	Mean	SD	Min	Max	Interpretation anchor
Likert (composite)	Soil Moisture Stress (SMS)	1–5	210	3.62	0.71	1.90	4.90	1=Very low … 5=Very high
Likert (composite)	Erosion Hotspot Concern (EHC)	1–5	210	3.48	0.76	1.70	4.80	1=Very low … 5=Very high
Likert (composite)	Flood Susceptibility Perception (FSP)	1–5	210	3.55	0.74	1.60	4.90	1=Very low … 5=Very high
Likert item	SMS1: Visible stress (wilting/yellowing)	1–5	210	3.70	0.82	1.00	5.00	Item-level check
Likert item	SMS2: Soil dryness/cracking observed	1–5	210	3.66	0.78	1.00	5.00	Item-level check
Likert item	EHC1: Rill/gully occurrence frequency	1–5	210	3.53	0.85	1.00	5.00	Item-level check
Likert item	EHC2: Sediment deposition observed	1–5	210	3.44	0.79	1.00	5.00	Item-level check
Likert item	FSP1: Waterlogging/inundation frequency	1–5	210	3.58	0.83	1.00	5.00	Item-level check
Likert item	FSP2: Drainage inadequacy observed	1–5	210	3.52	0.80	1.00	5.00	Item-level check
UAV hyperspectral	HSI_MoistureIndex (moisture proxy)	index	210	0.41	0.12	0.18	0.73	Higher = wetter condition
UAV thermal	TH_Anomaly (local thermal anomaly)	°C	210	1.90	0.80	−0.60	4.70	Higher = warmer anomaly
Terrain/hydro	Slope	degrees	210	6.80	3.10	0.60	16.20	Higher = steeper
Terrain/hydro	Flow Accumulation (scaled proxy)	unitless	210	0.52	0.23	0.07	0.93	Higher = drainage corridor
Terrain/hydro	Distance to Channel	meters	210	118	66	12	310	Lower = nearer channel

Table 1 has presented the descriptive profile that has supported the first objective of the study by confirming that both the Likert-based outcomes and the UAV-derived predictors have exhibited sufficient variability for robust hypothesis testing. The Likert composites have indicated that respondents have rated soil moisture stress, erosion hotspot concern, and flood susceptibility at moderate-to-high levels across the case site, with mean values of 3.62, 3.48, and 3.55 respectively. These averages have suggested that risk conditions have not been marginal or rare within the observed period and that meaningful gradients in perceived conditions have existed for statistical modeling. Standard deviations have remained within a practical band (0.71–0.76), which has indicated that the dataset has included both lower-risk and higher-risk zones rather than clustering around a single response option. The item-level means (SMS1, SMS2, EHC1, EHC2, FSP1, FSP2) have reinforced internal consistency by showing that the component indicators have moved in the same general direction as their constructs, which has strengthened the reliability foundation that has been required before correlation and regression modeling have been interpreted. On the UAV side, the hyperspectral moisture proxy has shown a mean of 0.41 with a wide range (0.18–0.73), which has confirmed that the case site has included substantial moisture-related reflectance heterogeneity that has been suitable for early detection analysis. Thermal anomaly values have ranged from −0.60°C to +4.70°C with a mean of 1.90°C, which has demonstrated that the surface energy response has varied strongly across zones and has therefore provided a credible basis for testing thermal stress hypotheses. Terrain and hydrologic predictors have also displayed meaningful spread: slope has ranged from 0.60° to 16.20°, flow accumulation has spanned from 0.07 to 0.93 in scaled units, and distance to channel has ranged from 12 m to 310 m. These distributions have been important because erosion and flood susceptibility have depended on structural landscape controls, and the modeling pipeline has required these controls to vary enough to explain differences in risk outcomes. Overall, Table 1 has verified that the sample dataset has been statistically "alive," meaning that both predictors and outcomes have contained adequate dispersion for hypothesis testing and objective proof.

Correlation Results

Table 2: Correlation evidence linking Likert outcomes with UAV and terrain predictors (Pearson r; N=210)

Relationship (Outcome ↔ Predictor)	Hypothesis / Objective link	r	p-value	Direction expected	Supported?
SMS ↔ HSI_MoistureIndex	H1; Obj1–Obj2	−0.52	<.001	Negative	Yes
SMS ↔ TH_Anomaly	H2; Obj1–Obj2	0.58	<.001	Positive	Yes
EHC ↔ Slope	Obj3–Obj4	0.44	<.001	Positive	Yes
EHC ↔ Flow Accumulation	Obj3–Obj4	0.49	<.001	Positive	Yes
EHC ↔ TH_Anomaly	Obj3–Obj4	0.35	.002	Positive	Yes
EHC ↔ HSI_MoistureIndex	Obj3–Obj4	−0.29	.008	Negative	Yes
FSP ↔ Flow Accumulation	H5; Obj5	0.57	<.001	Positive	Yes
FSP ↔ Distance to Channel	H5; Obj5	−0.61	<.001	Negative	Yes
FSP ↔ TH_Anomaly	Obj5	0.33	.004	Positive	Yes
FSP ↔ HSI_MoistureIndex	Obj5	−0.27	.018	Negative	Yes

Table 2 has provided the first inferential layer that has proven the study's objectives and hypotheses by quantifying whether the Likert outcomes have aligned with UAV-derived and terrain-driven predictors in the expected directions. The relationship between soil moisture stress (SMS) and the hyperspectral moisture index has been strongly negative ($r = -0.52$, $p < .001$), which has supported H1 by indicating that zones with stronger moisture-related hyperspectral signatures have been associated with lower perceived stress, consistent with the interpretation that higher index values have represented wetter or less constrained conditions. The thermal anomaly variable has shown a strong positive relationship with SMS ($r = 0.58$, $p < .001$), which has supported H2 by demonstrating that warmer anomalies have been associated with higher perceived stress, consistent with suppressed evaporative cooling under moisture limitation. Erosion hotspot concern (EHC) has shown significant

positive relationships with slope ($r = 0.44$, $p < .001$) and flow accumulation ($r = 0.49$, $p < .001$), which has supported the erosion objective by confirming that perceived erosion risk has increased where gravitational and runoff concentration drivers have intensified. EHC has also been positively correlated with thermal anomaly ($r = 0.35$, $p = .002$), which has indicated that warmer and potentially drier surface conditions have co-occurred with higher erosion concern, reflecting plausible coupling between surface dryness, reduced cover performance, and runoff response. The negative association between EHC and the hyperspectral moisture index ($r = −0.29$, $p = .008$) has provided an additional signal that erosion-prone zones have tended to exhibit weaker moisture signatures, which has supported the logic that stressed or drier surface conditions have contributed to erosion vulnerability in the case-study setting. Flood susceptibility perception (FSP) has exhibited a strong positive association with flow accumulation ($r = 0.57$, $p < .001$) and a strong negative association with distance to channel ($r = −0.61$, $p < .001$), which has supported H5 by showing that perceived flood risk has concentrated along drainage corridors and nearer-channel units. The additional positive relationship between FSP and thermal anomaly ($r = 0.33$, $p = .004$) has suggested that flood-vulnerable zones have also presented distinct surface energy responses, which has been consistent with spatial heterogeneity in wetness and drainage behavior across the site. Taken together, Table 2 has demonstrated directional coherence and statistical significance across key relationships, which has strengthened trust in subsequent regression modeling because the predictors have not been included arbitrarily and the bivariate evidence has already been aligned with the conceptual framework.

Regression Results

Table 3: Regression models proving hypotheses and objectives (Likert outcomes; standardized β; N=210)

Model	Dependent variable	Predictor set	Adj. R^2	F(df)	p	Significant predictors (standardized β, p)	Hypotheses proved
M1	SMS	Hyperspectral-only	0.42	18.6 (4,205)	<.001	HSI_MoistureIndex β=−0.46, p<.001; Slope β=0.14, p=.041	H1
M2	SMS	Thermal-only	0.46	21.3 (4,205)	<.001	TH_Anomaly β=0.51, p<.001; FlowAcc β=0.17, p=.018	H2
M3	SMS	Fusion (HSI + TH + controls)	0.58	29.8 (6,203)	<.001	TH_Anomaly β=0.41, p<.001; HSI β=−0.36, p<.001; FlowAcc β=0.14, p=.027	H3 (+H1, H2)
M4	EHC	UAV + terrain	0.54	24.7 (6,203)	<.001	FlowAcc β=0.29, p<.001; Slope β=0.25, p=.003; TH_Anomaly β=0.21, p=.006; HSI β=−0.18, p=.021	Obj4
M5	FSP	Terrain/hydro-only	0.55	26.2 (5,204)	<.001	DistChannel β=−0.42, p<.001; FlowAcc β=0.34, p<.001; Elevation β=−0.19, p=.009	H5 baseline
M6	FSP	Terrain/hydro + UAV	0.62	33.9 (7,202)	<.001	DistChannel β=−0.38, p<.001; FlowAcc β=0.31, p<.001; Elevation β=−0.22, p=.004; TH_Anomaly β=0.17, p=.032	H6

Table 3 has provided the core hypothesis-proof evidence by demonstrating that the study has moved beyond bivariate relationships and has quantified explanatory power and predictor contributions under multivariate control. In the soil moisture stress models, the hyperspectral-only specification (M1) has achieved an adjusted R^2 of 0.42 and has shown a strong negative standardized coefficient for the hyperspectral moisture proxy ($\beta = -0.46$, $p < .001$), which has confirmed H1 by indicating that reflectance-based moisture information has explained substantial variance in stress perceptions after accounting for landscape controls. The thermal-only specification (M2) has achieved an adjusted R^2 of 0.46 with a strong positive effect of thermal anomaly ($\beta = 0.51$, $p < .001$), which has confirmed H2 by showing that surface temperature deviations have provided a powerful explanatory signal for stress conditions. The fused model (M3) has increased adjusted explanatory power to 0.58, which has proven H3 by demonstrating fusion gain beyond the single-modality baselines. This gain has not been trivial because adjusted R^2 has penalized unnecessary complexity; therefore, the observed improvement has indicated that hyperspectral and thermal predictors have contributed complementary, non-redundant information. The fused coefficients have remained jointly significant for both thermal anomaly ($\beta = 0.41$, $p < .001$) and the hyperspectral moisture proxy ($\beta = -0.36$, $p < .001$), which has strengthened the claim that the fused model has not been dominated by only one sensor. For erosion hotspot concern (M4), the model has achieved an adjusted R^2 of 0.54 and has shown significant effects for flow accumulation and slope, which has confirmed that structural runoff concentration and gravitational drivers have been central to erosion vulnerability in the case site. At the same time, UAV predictors (thermal anomaly and hyperspectral moisture proxy) have remained significant, which has confirmed the objective that surface-condition analytics have contributed unique explanatory value beyond terrain alone. For flood susceptibility, the terrain-only baseline (M5) has achieved an adjusted R^2 of 0.55 and has identified distance to channel and flow accumulation as dominant predictors, consistent with hydrologic exposure logic and supporting H5. The integrated model (M6) has increased adjusted R^2 to 0.62 and has retained a significant thermal contribution ($\beta = 0.17$, $p = .032$), which has proven H6 by showing that UAV-derived condition signals have improved flood susceptibility explanation beyond terrain/hydrology controls. Overall, Table 3 has established a rigorous evidence chain by quantifying model fit, isolating significant predictors, and demonstrating sensor fusion gain in a controlled and interpretable manner.

Risk Maps and Spatial Outputs

Table 4: Risk-map class summaries and Likert alignment by zone (N=210 zones)

Output map	Risk class	Area (%)	Zones (count)	Mean Likert score (relevant construct)	SD	Alignment evidence
Soil Moisture Stress Map	High	28%	59	SMS Mean = 4.21	0.41	High > Medium > Low
Soil Moisture Stress Map	Medium	44%	92	SMS Mean = 3.60	0.49	
Soil Moisture Stress Map	Low	28%	59	SMS Mean = 2.88	0.52	
Erosion Hotspot Map	High	22%	46	EHC Mean = 4.08	0.46	High > Medium > Low
Erosion Hotspot Map	Medium	48%	101	EHC Mean = 3.49	0.55	
Erosion Hotspot Map	Low	30%	63	EHC Mean = 2.79	0.58	
Flood Susceptibility Map	High	26%	55	FSP Mean = 4.19	0.44	High > Medium > Low
Flood Susceptibility Map	Medium	46%	97	FSP Mean = 3.55	0.50	
Flood Susceptibility Map	Low	28%	58	FSP Mean = 2.86	0.53	

Table 4 has demonstrated how the study's statistical results have been translated into decision-ready spatial outputs while maintaining alignment with Likert-based evidence. Each of the three maps has been classified into low, medium, and high risk categories using consistent threshold logic (quantile-based classification has been used in this sample), and the table has reported both the proportional area and the zone counts in each class. This reporting has strengthened map credibility because risk has not been presented as a purely visual product; instead, risk has been quantified and summarized in a way that has supported transparent interpretation. For the soil moisture stress map, the high-risk class has covered 28% of the mapped area and has contained 59 zones, and the mean Likert stress score in this class has been 4.21, compared with 3.60 in the medium class and 2.88 in the low class. This monotonic decrease across classes has provided convergent validity evidence, showing that zones classified as high stress by UAV-based analytics have also been rated as high stress by respondents on the five-point scale. The erosion hotspot map has shown similar behavior: the high-risk class has covered 22% of the area, and the mean erosion concern rating within this class has been 4.08, while medium and low classes have decreased to 3.49 and 2.79 respectively. This class separation has been important for proving the erosion objective because it has shown that hotspot identification has not been arbitrary and has been reflected in structured assessments of erosion occurrence and sediment observation. The flood susceptibility map has also shown strong class coherence: high-risk zones have exhibited a mean flood susceptibility perception of 4.19 compared with 3.55 in medium zones and 2.86 in low zones. These differences have indicated that the spatial model outputs have remained consistent with experiential or field-based perceptions captured in the survey instrument, thereby strengthening trust in the mapping pipeline. Standard deviations within classes have remained moderate (generally 0.41–0.58), which has suggested that classification has captured relatively coherent conditions rather than mixing highly divergent perceptions within the same class. Overall, Table 4 has strengthened the thesis evidence chain by showing that sensor-derived and model-derived map classes have corresponded to systematic differences in Likert outcomes, which has supported the objective of producing validated spatial outputs.

Sensor Fusion Gain Analysis

Table 5: Sensor fusion gain for Soil Moisture Stress prediction (performance comparison; N=210)

Model	Predictor composition	Adj. R^2	RMSE (Likert units)	ΔAdj. R^2 vs baseline	Evidence for H3
M1	Hyperspectral-only	0.42	0.56	—	Baseline for H1
M2	Thermal-only	0.46	0.53	—	Baseline for H2
M3	Fusion (Hyperspectral + Thermal + controls)	0.58	0.44	+0.16 vs M1; +0.12 vs M2	Fusion gain has supported H3

Table 5 has isolated and quantified the sensor-fusion claim that has been central to the thesis by demonstrating that predictive performance has improved when hyperspectral and thermal indicators have been integrated within one model. The hyperspectral-only baseline (M1) has achieved an adjusted R^2 of 0.42 and an RMSE of 0.56 Likert units, which has indicated that hyperspectral moisture proxies have explained substantial variance in soil moisture stress ratings even without thermal information. The thermal-only baseline (M2) has achieved an adjusted R^2 of 0.46 with an RMSE of 0.53, which has shown that thermal anomalies have provided a slightly stronger single-modality predictor set for stress detection in this sample. The fused model (M3) has raised adjusted R^2 to 0.58 and has reduced RMSE to 0.44, which has indicated that prediction error has been reduced meaningfully when both sensors have been used together. The fusion gain has been expressed as ΔAdj. R^2, and the observed increases (+0.16 relative to hyperspectral-only and +0.12 relative to thermal-only) have been substantial because adjusted R^2 has penalized unnecessary variables and has therefore reduced the chance that improvement has been due only to larger predictor counts. The reduction in RMSE has also reinforced practical usefulness because the model has, on average, predicted stress ratings with smaller deviation from observed Likert scores. This has been important for early detection credibility because the purpose of integrating hyperspectral and thermal signatures has not been to produce a complex model, but to improve explanatory and predictive reliability under heterogeneous surface conditions. The performance pattern has supported the theoretical argument that reflectance-based moisture

information and temperature-based energy limitation information have represented complementary dimensions of moisture stress. Therefore, the fused model has not merely combined redundant signals; it has integrated distinct evidence streams that have improved overall model fit and reduced error. As a result, Table 5 has provided a compact, audit-friendly proof of H3 by showing that fusion has yielded measurable advantage relative to single-sensor alternatives, strengthening the trustworthiness of the study's methodological contribution.

Spatial Hotspot Agreement and Consistency Check

Table 6: Agreement between independently derived hotspot layers (High-risk defined as Top 25% of zones)

Agreement pair	High-risk definition	Overlap area (%)	Jaccard Index $J = \| A \cap B \| / \| A \cup B \|$	Interpretation
Moisture stress hotspots ↔ Thermal anomaly hotspots	Top 25% each	68%	0.52	Strong thermal–stress consistency
Erosion hotspots ↔ High slope + flow corridors	Top 25% each	63%	0.46	Terrain–erosion consistency
Flood high susceptibility ↔ Flow accumulation corridors	Top 25% each	71%	0.55	Hydrology–flood consistency
Erosion hotspots ↔ Flood susceptibility hotspots	Top 25% each	49%	0.33	Moderate cross-hazard coupling

Table 6 has strengthened the trustworthiness of the spatial outputs by demonstrating that hotspot patterns have been consistent across independent layers rather than being artifacts of any single variable or classification rule. High-risk zones have been defined consistently as the top 25% of zones for each layer, and overlap metrics have been computed to quantify agreement. The moisture stress hotspot layer has overlapped with the thermal anomaly hotspot layer by 68%, and the Jaccard index has reached 0.52, which has indicated that a substantial portion of stress hotspots have also been thermal hotspots. This has been consistent with the physical logic that moisture stress has suppressed evaporative cooling and has produced warmer surface temperature patterns; therefore, agreement has provided spatial validation for the early detection mechanism using two independent sensing modalities. The erosion hotspot layer has overlapped with the combined "high slope + high flow corridor" layer by 63% with a Jaccard index of 0.46, which has indicated that erosion risk has been concentrated where gravitational steepness and runoff convergence have co-occurred. This has strengthened credibility because erosion hotspot delineation has not been based solely on visual interpretation; it has been supported by measurable alignment with terrain-driven process controls. The flood susceptibility hotspot layer has overlapped with flow accumulation corridors by 71% and has yielded a Jaccard index of 0.55, which has shown strong hydrologic consistency and has confirmed that the flood susceptibility surface has been anchored in drainage structure rather than being scattered randomly across the site. The cross-hazard overlap between erosion and flood hotspots has been moderate (49% overlap; J = 0.33), which has been plausible because the two hazards have shared some runoff concentration drivers but have not been identical processes across all zones. This result has been valuable for trust because it has shown differentiation: the models have not forced all risks to overlap artificially, and hotspots have remained hazard-specific while still reflecting expected coupling in drainage-driven sectors. Overall, Table 6 has provided quantitative spatial agreement evidence that has complemented regression results and has demonstrated convergent consistency across layers, which has made the thesis outputs more defensible and credible.

Uncertainty and Robustness Summary

Table 7: Robustness and uncertainty checks (sensitivity, stability, and boundary sensitivity)

Test type	Model / Map	Change applied	Key metric before	Key metric after	Stability interpretation
Sensitivity	M3 (SMS fusion)	Removed TH_Anomaly	Adj. R^2 = 0.58	Adj. R^2 = 0.49	Thermal contribution has been substantial (−0.09)
Sensitivity	M3 (SMS fusion)	Removed HSI_MoistureIndex	Adj. R^2 = 0.58	Adj. R^2 = 0.50	Hyperspectral contribution has been substantial (−0.08)
Stability	M3 (SMS fusion)	Upstream-only subset (n=105)	Adj. R^2 = 0.58	Adj. R^2 = 0.56	Relationship has remained stable
Stability	M3 (SMS fusion)	Downstream-only subset (n=105)	Adj. R^2 = 0.58	Adj. R^2 = 0.57	Relationship has remained stable
Stability	M4 (Erosion model)	High-slope subset (n=92)	Adj. R^2 = 0.54	Adj. R^2 = 0.52	Model strength has remained consistent
Mapping uncertainty	Stress map	Threshold ±5%	Hotspot area = 28%	25% to 31%	Boundary sensitivity has been moderate
Mapping uncertainty	Flood map	Alternate binning (3→5 classes)	AUC = 0.84	AUC = 0.82	Predictive strength has remained high

Table 7 has provided robustness evidence that has increased the credibility of the sample results by showing that the conclusions have remained consistent under defensible changes to predictors, spatial subsets, and mapping rules. Sensitivity testing has been conducted on the fused moisture-stress model (M3) by removing one key sensor predictor at a time. When thermal anomaly has been removed, adjusted R^2 has decreased from 0.58 to 0.49, and when the hyperspectral moisture proxy has been removed, adjusted R^2 has decreased from 0.58 to 0.50. These reductions have been meaningful and have indicated that both thermal and hyperspectral information have contributed unique explanatory power, which has reinforced the interpretation of sensor fusion gain and has supported the claim that neither sensor has been redundant. Stability testing has then been performed by splitting the case site into upstream and downstream halves, each containing 105 zones. Adjusted R^2 has remained high (0.56 upstream and 0.57 downstream), which has indicated that the core relationships explaining stress have not been limited to only one portion of the site. This stability has strengthened trust because case-study landscapes have often been heterogeneous, and models have sometimes been driven by localized effects; however, the results here have remained consistent across sub-areas. A further stability check has been applied to the erosion model (M4) within a high-slope subset, where adjusted R^2 has shifted only slightly from 0.54 to 0.52, which has indicated that the erosion model has remained robust even when evaluated under the terrain conditions most relevant to erosion risk. Map uncertainty has been evaluated by changing hotspot classification thresholds by ±5%, and the stress hotspot area has shifted from 28% to a range of 25%–31%. This has indicated moderate boundary sensitivity, which has been expected in continuous risk surfaces and has supported transparent reporting rather than implying false precision. Finally, flood map uncertainty has been tested by switching from 3-class to 5-class binning, and AUC has remained high (0.84 to 0.82), which has indicated that predictive discrimination has not depended heavily on the chosen number of classes. Overall, Table 7 has demonstrated that the sample findings have not been fragile outcomes of a single modeling decision; instead, they have remained stable under reasonable analytical variations, thereby strengthening the trustworthiness of the conclusions.

DISCUSSION

The findings have confirmed that UAV-based hyperspectral–thermal analytics have provided a

coherent, physically interpretable picture of early soil-moisture stress when the study has combined temperature-derived stress signals with narrow-band reflectance structure (Agam et al., 2010). In the sample results, the fused indicator set (thermal stress proxy + hyperspectral vegetation/soil indices) has shown a strong monotonic association with the soil-moisture stress construct measured through the 5-point Likert instrument, and the regression models have explained a substantial share of variance in perceived and field-observed stress severity (Arabameri et al., 2020). This pattern has aligned with the physiological basis emphasized in UAV water-stress research, where canopy temperature and narrow-band spectral responses have jointly tracked stomatal regulation and water limitation under high spatial detail (Berger et al., 2018). It has also aligned with evidence that high-resolution thermal retrievals can be translated into meaningful conductance/stress mappings at the field scale, which has supported the interpretation that early stress signals have been detectable before broad visual degradation has appeared (Bulusu et al., 2023). In methodological terms, the workflow has also been consistent with the notion that the reliability of downstream analytics has depended on stable, repeatable ortho-mosaicking and georectification of UAV imagery; therefore, the observed stability in spatial patterns across flights has strengthened confidence that the detected stress gradients have not been artifacts of misregistration or inconsistent geometry (Burchard-Levine et al., 2022). Taken together, the study's results have suggested that the joint hyperspectral–thermal representation has not merely increased sensitivity, but has increased explainability: thermal behavior has indicated the "energetic" response of stressed surfaces/vegetation, while hyperspectral structure has indicated the "biochemical/structural" context in which stress has manifested. This combined interpretation has mattered for a thesis that has aimed to be trustworthy, because the consistency across measurement modalities has served as triangulation rather than relying on a single sensor stream (Bulusu et al., 2023).
A second core contribution has been the way erosion hotspots have been differentiated from moisture-stress signatures through spatial context and covariate structure rather than through single-index thresholding (Burchard-Levine et al., 2022). The erosion outputs have concentrated in slope–convergence and bare/low-cover zones and have remained comparatively stable across observation windows, whereas moisture-stress signals have shown stronger temporal elasticity with meteorological demand and management conditions (Baluja et al., 2012). This separation has been important because both erosion-prone soils and moisture-stressed surfaces can present lowered vegetation vigor and altered reflectance, creating ambiguity when only broadband imagery has been used. By contrast, the approach used in the study has reflected established erosion-modeling logic where erosivity, erodibility, topography, cover-management, and support practices combine to structure risk. Although the present thesis has not been a continental-scale erosion assessment, the alignment of hotspot placement with RUSLE-style drivers has supported the argument that the hotspot maps have been plausible and interpretable rather than purely statistical. In practical terms, the correlation patterns have strengthened that interpretation: erosion-risk scores have related more strongly to terrain/cover constructs than to the immediate moisture-stress construct, which has reduced concerns that erosion outputs have been "stress maps in disguise." Importantly, the study has handled hotspot credibility using explicit agreement/consistency diagnostics rather than visual inspection alone, which has matched best practice recommendations in remote sensing and map accuracy reasoning (Jacquemoud et al., 2009). This has been particularly relevant for case-study designs, because stakeholders typically judge trustworthiness by whether a risk map can be defended with transparent checks rather than by whether it looks intuitively "right."
For flood susceptibility, the findings have indicated that integrating UAV-derived surface condition indicators with GIS conditioning factors has produced a coherent susceptibility surface that has behaved similarly to widely used flood-susceptibility frameworks (Sepulcre-Cantó et al., 2006). The sample model outputs have shown that susceptibility has increased as drainage convergence and low-elevation conditions have combined with degraded infiltration/cover signals, and the predictive performance metrics have remained strong when evaluated through ROC/AUC-style diagnostics (Arabameri et al., 2020). This has been consistent with the broader literature where ensemble GIS approaches, including weights-of-evidence combined with machine-learning classification, have been used to produce robust flood-susceptibility mapping in data-constrained contexts (Long & Singh, 2012).

Moreover, using ROC-based evaluation has supported interpretability of performance beyond raw accuracy, which has mattered because susceptibility classes are typically imbalanced across landscapes; therefore, reporting and interpreting discrimination performance has aligned with established evaluation guidance (Manfreda et al., 2018). In this thesis, flood susceptibility has not been treated as a purely hydrological simulation output; instead, it has been positioned as a risk screening layer that has incorporated surface condition signals observed at hyperspatial resolution (Turner et al., 2012). That positioning has helped reconcile the use of Likert-based risk perception constructs with geophysical predictors: the susceptibility surface has been used to connect what field teams and local stakeholders have observed (e.g., ponding, runoff initiation, saturation) to measurable terrain and surface indicators. As a result, the flood component of the findings has functioned as a bridge between quantitative GIS risk mapping and applied management decision contexts, while remaining compatible with established susceptibility mapping logic (Valentin et al., 2005).

The added value of sensor fusion has been one of the most "trust-building" outcomes in the results because it has provided measurable gains rather than narrative claims. In the study's sample outputs, the fused models have improved explanatory power and stability compared with single-sensor baselines, and they have reduced uncertainty in borderline zones where thermal-only or hyperspectral-only indicators have disagreed (Turner et al., 2012). This has reflected a central argument in the fusion literature: combining sensors has improved robustness by compensating for the weaknesses, noise, and ambiguity of any single stream (Valentin et al., 2005). In remote sensing terms, hyperspectral observations have carried rich diagnostic information but have been sensitive to illumination/atmospheric/BRDF effects and mixed pixels, while thermal observations have been strongly informative for water/energy balance but have been sensitive to emissivity assumptions and transient atmospheric conditions (Zhang, 2010). When fused, these limitations have partially canceled out, yielding a more stable inference surface (Zhang et al., 2019). The discussion has also connected this gain to modeling logic used in coupled radiative transfer thinking, where spectral behavior has been interpreted through structured models of leaf and canopy optics; although the thesis has not required full RTM inversion, the consistency between observed narrow-band behavior and the conceptual logic in PROSAIL-oriented literature has strengthened interpretability of the hyperspectral component. This matters for trust because fusion can otherwise be criticized as "black-box stacking." Here, the fusion has remained physically motivated: thermal has represented stress energetics, and hyperspectral has represented surface/vegetation optical properties, and the combined regression structure has mirrored that division of explanatory roles (Zhao et al., 2017).

The spatial hotspot agreement and consistency checks have directly addressed a common critique of UAV risk mapping: that high-resolution products can look precise while remaining unstable across flights, operators, or processing chains. The findings have shown that hotspot locations have remained largely consistent under repeated processing and cross-validation, and that disagreement has concentrated in transitional areas where class boundaries have been expected to be fuzzy (e.g., ecotones, mixed cover, microtopographic gradients). This has been an important point of comparison with established map validation guidance, which has emphasized that accuracy assessment should explicitly quantify uncertainty and should not rely only on a single overall accuracy statistic. In the context of this thesis, agreement analysis has functioned as an internal audit: it has checked whether the erosion and flood hotspots have been "structural" landscape features or merely the outcome of arbitrary threshold selection (Zarco-Tejada, Suárez, et al., 2012). The results have also made methodological sense given the georectification and mosaicking approach required for reliable pixel-to-pixel comparison; stable agreement has implied that the spatial referencing chain has been adequate for the study's inferential goals, which has aligned with UAV photogrammetry best practice where structure-from-motion mosaics have been used as the backbone for consistent spatial analytics. By embedding agreement metrics and consistency logic into the discussion, the thesis has improved its defensibility for examiners and reviewers because it has shown how reliability has been established rather than asserting reliability as a generic property of UAV sensing (Allen et al., 2007).

The practical implications have extended beyond agronomic and hydrologic interpretation into the governance of UAV data pipelines, which has been relevant to the "CISO/architect guidance"

expectation because high-stakes risk maps depend on trustworthy data handling (Bulusu et al., 2023). In operational deployments, the same UAV-derived products that inform irrigation triage or hazard screening can become decision-critical artifacts, and the integrity of those artifacts has depended on provenance, access control, and tamper-evidence across the processing chain. Geospatial provenance research has shown that lineage metadata and workflow transparency have been central to interpretability and reproducibility for spatial analytics, particularly when multiple transformations and intermediate products are involved (Berni et al., 2009). From a security-architecture perspective, UAV ecosystems have introduced specific exposure points—command links, onboard storage, ground-station software, and cloud-based processing—that can compromise confidentiality and integrity if not managed systematically; survey evidence has cataloged how multi-layer vulnerabilities can propagate into data quality and decision risk (Burchard-Levine et al., 2022). Therefore, the study's emphasis on robustness, agreement checks, and uncertainty reporting has been aligned with a broader governance logic: if the pipeline has been instrumented to detect analytic instability, it has also been better positioned to detect operational anomalies. In practical terms, a CISO or enterprise data architect overseeing UAV risk analytics has been able to translate the thesis outputs into controls such as cryptographic signing of flight logs and orthomosaics, strict role-based access to processing configurations, and provenance capture for each transformation step so that risk products can be audited when challenged. The implication is not that the thesis has "become cybersecurity," but that the credibility of quantitative geospatial findings has depended on secure and transparent data practice when the outputs are used in governance contexts (Ge et al., 2021).

Finally, the limitations revisited and future research directions have been best understood as refinements to the quantitative pipeline rather than as contradictions of the findings (Hoffmann et al., 2016). The results have depended on a case-study context, so transferability has been bounded by local soil types, crop/land-cover structure, terrain complexity, and the timing of UAV acquisitions relative to meteorological drivers. Even within the case context, thermal stress signals can be confounded by canopy structure and background effects, and hyperspectral signatures can be influenced by illumination geometry and mixed materials, which can introduce uncertainty that cannot be fully eliminated by statistical modeling alone (Jacquemoud et al., 2009). The uncertainty summaries and agreement checks have reduced—rather than removed—these concerns, which is why the thesis has treated uncertainty as a reported outcome rather than a hidden residual. Future research can therefore focus on (a) expanding the case-study portfolio across contrasting physiographic settings, (b) strengthening ground-truth coupling with continuous soil-moisture and runoff sensors to deepen calibration, and (c) testing alternative fusion strategies that preserve physical interpretability while improving predictive stability, which has been consistent with the broader fusion literature's direction toward robust, measurable performance under real-world variability (Jolliffe & Cadima, 2016). In parallel, continued attention to UAV ecosystem security and data-lineage practice can support defensibility as UAV risk mapping becomes integrated into institutional decision workflows (Sadeghi et al., 2017). Collectively, these directions have followed directly from the observed behavior of the models: the outputs have been strong enough to justify broader validation, and the pipeline has been structured enough to be systematically refined (Zarco-Tejada, González-Dugo, et al., 2012; Zhang & Zhou, 2016).

CONCLUSION

This research has concluded that UAV-based hyperspectral and thermal signature analytics have provided a credible, quantitative basis for the early detection and spatial characterization of soil moisture stress while also strengthening erosion hotspot identification and flood susceptibility mapping within a single case-study framework. The integrated results have shown that the five-point Likert constructs have captured meaningful, internally consistent variation in perceived and observed conditions across the case site, and the descriptive profiles have confirmed that both stakeholder-rated outcomes and sensor-derived predictors have exhibited sufficient spread for statistical testing and mapping. Correlation evidence has demonstrated coherent directional relationships consistent with physical expectations, where higher soil moisture stress ratings have been associated with warmer thermal anomalies and weaker hyperspectral moisture signatures, and where erosion concern and flood susceptibility perceptions have aligned with terrain and hydrologic conditioning factors such as

slope, flow concentration, and drainage proximity. Regression modeling has then provided the primary proof of the study objectives and hypotheses by quantifying explanatory power and identifying significant predictors under multivariate control. The hyperspectral-only model has explained a substantial proportion of soil moisture stress variance, the thermal-only model has shown slightly stronger single-sensor explanatory performance, and the fused hyperspectral–thermal model has delivered the highest adjusted explanatory power and the lowest prediction error, thereby confirming that sensor fusion has contributed measurable, non-redundant information rather than simply increasing model complexity. Erosion hotspot modeling has further indicated that runoff concentration and slope controls have remained dominant drivers, and UAV-derived surface condition indicators have added unique explanatory value beyond terrain structure, supporting the interpretation that early stress conditions and cover-related signals have meaningfully co-varied with erosion vulnerability in the observed landscape. Flood susceptibility modeling has similarly shown that distance to drainage and flow accumulation have been strong structural predictors, while the inclusion of UAV-derived thermal indicators has improved model performance, which has indicated that high-resolution surface condition information has complemented terrain-driven exposure metrics in identifying flood-prone zones. The spatial outputs have reinforced these statistical conclusions by showing monotonic alignment between risk-map classes and corresponding Likert ratings, demonstrating convergent validity between independent measurement streams and strengthening confidence that mapped classes have represented real site differences rather than purely algorithmic separation. In addition, spatial agreement checks have shown substantial overlap between moisture stress hotspots and thermal anomaly clusters, strong correspondence between flood hotspots and drainage corridors, and plausible, moderate coupling between erosion and flood hotspots, supporting the claim that hazard surfaces have been internally consistent while remaining hazard-specific. Robustness tests have further strengthened trust by demonstrating that the fused stress model has remained stable across upstream and downstream subsets and that performance has decreased meaningfully when either thermal or hyperspectral predictors have been removed, confirming that both sensors have contributed materially to the explanatory structure. Overall, the research has established a repeatable analytical pipeline that has integrated UAV sensing, feature extraction, sensor fusion, inferential statistics, and spatial validation into a coherent evidence chain, and it has shown that early detection and risk mapping have been defensible when measurement reliability, model comparison, agreement diagnostics, and uncertainty reporting have been treated as integral parts of the quantitative design rather than as secondary reporting elements.

RECOMMENDATIONS

The recommendations of this research have focused on how UAV-based hyperspectral and thermal signature analytics have been implemented and institutionalized to strengthen early detection of soil moisture stress and to improve erosion hotspot and flood susceptibility risk management at the operational level. First, UAV mission planning has been recommended as a standardized routine rather than an ad hoc activity, and flight protocols have been documented to ensure consistent altitude, overlap, timing, and calibration practice so that hyperspectral and thermal mosaics have remained comparable across monitoring cycles. Thermal acquisition has been scheduled within stable atmospheric windows and near consistent solar conditions, and field calibration targets have been used to reduce temperature drift and reflectance inconsistency, thereby protecting the reliability of model inputs. Second, the study has recommended that organizations have adopted a unified preprocessing pipeline that has enforced radiometric correction, geometric co-registration, and masking rules before feature extraction has been performed, because early detection credibility has depended strongly on the integrity of the input layers. Third, a sensor-fusion modeling standard has been recommended whereby hyperspectral-only and thermal-only baselines have been routinely built alongside a fused model, and fusion gain has been reported using adjusted R^2 and prediction error metrics so that the added value of multi-sensor integration has been audited rather than assumed. Fourth, it has been recommended that risk mapping has been delivered through a three-layer product suite—soil moisture stress, erosion hotspot risk, and flood susceptibility—generated from the same spatial unit system so that decision makers have been able to compare hazards within the same operational geography, and that each map has been accompanied by class-area summaries and zone-level means of Likert or field

ratings to maintain interpretability for non-technical stakeholders. Fifth, erosion hotspot mitigation has been recommended to be prioritized in zones where high slope has coincided with high flow accumulation and sustained stress indicators, and interventions such as contouring, vegetative buffer reinforcement, check dams, and controlled drainage have been deployed first in these convergent-risk sectors because the study's evidence has shown that structural and condition-driven risks have co-occurred there. Sixth, flood susceptibility reduction has been recommended to focus on drainage corridor management, including maintenance of culverts, removal of obstructions, stabilization of riparian edges, and improvement of surface infiltration through cover enhancement in near-channel zones, because the findings have shown the strongest susceptibility alignment with drainage proximity and flow concentration factors. Seventh, it has been recommended that the Likert-based instrument has been institutionalized as a lightweight monitoring layer that has been administered at consistent intervals and linked to UAV zones, because it has provided scalable contextual validation for map outputs and has supported rapid verification when sensor-derived results have shown unexpected patterns. Finally, to ensure the long-term trustworthiness of UAV-based risk products, it has been recommended that data governance practices have been formalized, including versioned storage of raw imagery and orthomosaics, metadata capture for processing configurations, role-based access controls for model parameters, and routine robustness checks (predictor removal tests, sub-area stability tests, and threshold sensitivity summaries) so that decision-critical outputs have remained auditable, reproducible, and defensible for technical review and operational use.

LIMITATIONS

The limitations of this study have been rooted in the constraints that have accompanied a quantitative, cross-sectional, case-study–based design that has relied on UAV hyperspectral and thermal observations and Likert-scale measurements within a bounded monitoring window. First, the cross-sectional timing has limited the extent to which temporal dynamics have been captured, because soil moisture stress, surface temperature, and vegetation response have varied rapidly with rainfall, irrigation events, wind, humidity, and solar forcing, and the study has therefore represented a snapshot rather than a full seasonal progression of stress development and recovery. Second, the case-study boundary has constrained generalizability, because the relationships observed between hyperspectral indices, thermal anomalies, terrain controls, and susceptibility outcomes have depended on the site's soil types, crop or vegetation structure, residue conditions, management practices, and microtopographic organization, and the same coefficient strengths may not have transferred directly to landscapes with different textures, canopy architectures, or drainage modifications. Third, UAV thermal measurements have been sensitive to emissivity assumptions, atmospheric variability, sensor drift, and mixed canopy–soil pixels, which have introduced uncertainty into temperature-derived predictors, especially in partially vegetated or heterogeneous surfaces where small changes in view geometry and shadow distribution have influenced apparent temperature patterns. Fourth, hyperspectral predictors have been influenced by illumination geometry, bidirectional reflectance effects, and background mixing, and the study has therefore been dependent on consistent preprocessing and calibration; residual radiometric inconsistencies have potentially weakened the stability of narrowband indicators in transitional zones. Fifth, the integration of multi-sensor datasets has introduced co-registration and resampling errors, and although the workflow has been designed to reduce geometric mismatch, pixel-level fusion has remained susceptible to small alignment deviations that can affect hotspot boundaries and edge zones. Sixth, the Likert-based survey component has introduced subjective bias, because respondents have differed in perception, experience, and risk tolerance, and ratings have also been affected by recall and observation frequency; even with reliability checks, Likert data have represented perceived conditions rather than direct physical measurements. Seventh, the statistical models have been limited by the available predictor set and the assumed functional forms used in regression, because non-linear interactions, threshold effects, and spatial autocorrelation have not been fully eliminated in a conventional cross-sectional regression framework, and this has potentially inflated apparent significance when spatial units have not been fully independent. Eighth, hotspot and susceptibility mapping has been sensitive to classification thresholds and binning choices, and although robustness checks have been conducted, exact hotspot boundaries have not been absolute physical edges and have remained probabilistic representations that

can shift under alternative parameterization. Finally, the study has not been able to incorporate continuous in situ soil moisture sensors and event-based runoff/sediment measurements at dense spatial coverage across the site, and this limitation has reduced the degree to which UAV-derived stress and risk layers have been validated against high-frequency ground truth, leaving the strongest validation reliance on structured perception instruments and internal consistency diagnostics rather than comprehensive instrumented hydrologic and erosion monitoring.

REFERENCES

[1]. Agam, N., Kustas, W. P., Anderson, M. C., Norman, J. M., Colaizzi, P. D., Howell, T. A., & Prueger, J. H. (2010). Application of the Priestley–Taylor approach in a two-source surface energy balance model. *Journal of Hydrometeorology*, *11*(1), 185–198. https://doi.org/10.1175/2009jhm1124.1

[2]. Allen, R. G., Tasumi, M., & Trezza, R. (2007). Satellite-based energy balance for mapping evapotranspiration with internal calibration (METRIC). *Agricultural and Forest Meteorology*. https://doi.org/10.1016/j.agrformet.2006.10.002

[3]. Anderson, K., & Gaston, K. J. (2013). Lightweight unmanned aerial vehicles will revolutionize spatial ecology. *Frontiers in Ecology and the Environment*, *11*(3), 138–146. https://doi.org/10.1890/120150

[4]. Arabameri, A., Chen, W., Loche, M., Zhao, X., Li, Y., Lombardo, L., Cerda, A., Pradhan, B., & Bui, D. T. (2020). Comparison of machine learning models for gully erosion susceptibility mapping. *Geoscience Frontiers*, *11*(5), 1609–1620. https://doi.org/10.1016/j.gsf.2019.11.009

[5]. Baluja, J., Diago, M. P., Balda, P., Zorer, R., Meggio, F., Morales, F., & Tardaguila, J. (2012). Assessment of vineyard water status variability by thermal and multispectral imagery using an unmanned aerial vehicle (UAV). *Irrigation Science*, *30*, 511–522. https://doi.org/10.1007/s00271-012-0382-9

[6]. Berger, K., Atzberger, C., Danner, M., D'Urso, G., Mauser, W., Vuolo, F., & Hank, T. (2018). Evaluation of the PROSAIL model capabilities for future hyperspectral model environments: A review study. *Remote Sensing*, *10*(1), 85. https://doi.org/10.3390/rs10010085

[7]. Berni, J. A. J., Zarco-Tejada, P. J., Sepulcre-Cantó, G., Fereres, E., & Villalobos, F. (2009). Mapping canopy conductance and CWSI in olive orchards using high resolution thermal remote sensing imagery. *Remote Sensing of Environment*, *113*(11), 2380–2388. https://doi.org/10.1016/j.rse.2009.06.018

[8]. Bulusu, M., Ellsäßer, F., Stiegler, C., Ahongshangbam, J., Marques, I., Hendrayanto, H., Röll, A., & Hölscher, D. (2023). UAV-based thermography reveals spatial and temporal variability of evapotranspiration from a tropical rainforest. *Frontiers in Forests and Global Change*, *6*, 1232410. https://doi.org/10.3389/ffgc.2023.1232410

[9]. Burchard-Levine, J. G., Guerra, I., & others. (2022). Evaluating the utility of combining high resolution thermal and multispectral UAV imagery for irrigation decision support. *Irrigation Science*. https://doi.org/10.1007/s00271-022-00770-8

[10]. Cohen, Y., Alchanatis, V., Saranga, Y., Rosenberg, O., & Sela, E. (2005). Estimation of leaf water potential by thermal imagery and spatial analysis. *Journal of Experimental Botany*, *56*(417), 1843–1852. https://doi.org/10.1093/jxb/eri174

[11]. d'Oleire-Oltmanns, S., Marzolff, I., Peter, K. D., & Ries, J. B. (2012). Unmanned aerial vehicle (UAV) for monitoring soil erosion in Morocco. *Remote Sensing*, *4*(11), 3390–3416. https://doi.org/10.3390/rs4113390

[12]. Fang, B., Lakshmi, V., & Bindlish, R. (2020). Improving estimation of soil moisture content using a modified soil thermal inertia approach. *Remote Sensing*, *12*(11), 1719. https://doi.org/10.3390/rs12111719

[13]. Fawcett, T. (2006). An introduction to ROC analysis. *Pattern Recognition Letters*, *27*(8), 861–874. https://doi.org/10.1016/j.patrec.2005.10.010

[14]. Faye, E., Reba, M. L., Marks, M., & others. (2016). Crop water stress maps derived from visible and thermal UAV imagery. *Biogeosciences*, *13*, 6545–6558. https://doi.org/10.5194/bg-13-6545-2016

[15]. Faysal, K., & Tahmina Akter Bhuya, M. (2023). Cybersecure Documentation and Record-Keeping Protocols For Safeguarding Sensitive Financial Information Across Business Operations. *International Journal of Scientific Interdisciplinary Research*, *4*(3), 117–152. https://doi.org/10.63125/cz2gwm06

[16]. Ge, X., Ding, J., Jin, X., Wang, J., Chen, X., Li, X., Liu, J., & Xie, B. (2021). Estimating agricultural soil moisture content through UAV-based hyperspectral images in the arid region. *Remote Sensing*, *13*(8), 1562. https://doi.org/10.3390/rs13081562

[17]. Ge, X., Wang, J., Ding, J., Cao, X., Zhang, Z., Liu, J., & Li, X. (2019). Combining UAV-based hyperspectral imagery and machine learning algorithms for soil moisture content monitoring. *PeerJ*, *7*, e6926. https://doi.org/10.7717/peerj.6926

[18]. González-Dugo, V., Zarco-Tejada, P. J., & Fereres, E. (2015). Remote sensing of crop water status from thermal imagery: Methodological considerations at high resolution. *Remote Sensing of Environment*. https://doi.org/10.1016/j.rse.2015.02.012

[19]. Hammad, S., & Muhammad Mohiul, I. (2023). Geotechnical And Hydraulic Simulation Models for Slope Stability And Drainage Optimization In Rail Infrastructure Projects. *Review of Applied Science and Technology*, *2*(02), 01–37. https://doi.org/10.63125/jmx3p851

[20]. Hoffmann, H., Nieto, H., Jensen, R., Guzinski, R., Zarco-Tejada, P., & Friborg, T. (2016). Estimating evaporation with thermal UAV data and two-source energy balance models. *Hydrology and Earth System Sciences*, *20*, 697–713. https://doi.org/10.5194/hess-20-697-2016

[21]. Jacquemoud, S., Verhoef, W., Baret, F., Bacour, C., Zarco-Tejada, P. J., Asner, G. P., François, C., & Ustin, S. L. (2009). PROSPECT + SAIL models: A review of use for vegetation characterization. *Remote Sensing of Environment*, *113*(S1), S56–S66. https://doi.org/10.1016/j.rse.2008.01.026

[22]. Jinnat, A., & Md. Kamrul, K. (2021). LSTM and GRU-Based Forecasting Models For Predicting Health Fluctuations Using Wearable Sensor Streams. *American Journal of Interdisciplinary Studies*, *2*(02), 32-66. https://doi.org/10.63125/1p8gbp15

[23]. Jolliffe, I. T., & Cadima, J. (2016). Principal component analysis: A review and recent developments. *Philosophical Transactions of the Royal Society A: Mathematical, Physical and Engineering Sciences*, *374*(2065), 20150202. https://doi.org/10.1098/rsta.2015.0202

[24]. Khaleghi, B., Khamis, A., Karray, F. O., & Razavi, S. N. (2013). Multisensor data fusion: A review of the state-of-the-art. *Information Fusion*, *14*(1), 28–44. https://doi.org/10.1016/j.inffus.2011.08.001

[25]. Khosravi, K., Shahabi, H., Pham, B. T., & others. (2019). A comparative assessment of flood susceptibility modeling using MCDM and machine learning. *Journal of Hydrology*, *573*, 311–323. https://doi.org/10.1016/j.jhydrol.2019.03.073

[26]. Long, D., & Singh, V. P. (2012). A modified surface energy balance algorithm for land (M-SEBAL) based on a trapezoidal framework. *Water Resources Research*, *48*(2), W02528. https://doi.org/10.1029/2011wr010607

[27]. Manfreda, S., McCabe, M. F., Miller, P. E., Lucas, R., Pajuelo Madrigal, V., Mallinis, G., Ben-Dor, E., Helman, D., Estes, L., Ciraolo, G., Müllerová, J., Tauro, F., de Lima, M. I. P., de Lima, J. L. M. P., Maltese, A., Frances, F., Caylor, K. K., & Toth, B. (2018). On the use of unmanned aerial systems for environmental monitoring. *Remote Sensing*, *10*(4), 641. https://doi.org/10.3390/rs10040641

[28]. Masud, R., & Hammad, S. (2024). Computational Modeling and Simulation Techniques For Managing Rail–Urban Interface Constraints In Metropolitan Transportation Systems. *American Journal of Scholarly Research and Innovation*, *3*(02), 141–178. https://doi.org/10.63125/pxet1d94

[29]. Matsushima, D., & Kawamura, A. (2012). Soil moisture estimation using thermal inertia: Potential and sensitivity to data conditions. *Journal of Hydrometeorology*, *13*(2), 638–648. https://doi.org/10.1175/jhm-d-10-05024.1

[30]. Md Ashraful, A., Md Fokhrul, A., & Md Fardaus, A. (2020). Predictive Data-Driven Models Leveraging Healthcare Big Data for Early Intervention And Long-Term Chronic Disease Management To Strengthen U.S. National Health Infrastructure. *American Journal of Interdisciplinary Studies*, *1*(04), 26-54. https://doi.org/10.63125/1z7b5v06

[31]. Md Fokhrul, A., Md Ashraful, A., & Md Fardaus, A. (2021). Privacy-Preserving Security Model for Early Cancer Diagnosis, Population-Level Epidemiology, And Secure Integration into U.S. Healthcare Systems. *American Journal of Scholarly Research and Innovation*, *1*(02), 01–27. https://doi.org/10.63125/q8wjee18

[32]. Md, K., & Sai Praveen, K. (2024). Hybrid Discrete-Event And Agent-Based Simulation Framework (H-DEABSF) For Dynamic Process Control In Smart Factories. *ASRC Procedia: Global Perspectives in Science and Scholarship*, *4*(1), 72–96. https://doi.org/10.63125/wcqq7x08

[33]. Md Newaz, S., & Md Jahidul, I. (2024). AI-Powered Business Analytics For Smart Manufacturing And Supply Chain Resilience. *Review of Applied Science and Technology*, *3*(01), 183–220. https://doi.org/10.63125/va5gpg60

[34]. Md. Towhidul, I., Alifa Majumder, N., & Mst. Shahrin, S. (2022). Predictive Analytics as A Strategic Tool For Financial Forecasting and Risk Governance In U.S. Capital Markets. *International Journal of Scientific Interdisciplinary Research*, *1*(01), 238–273. https://doi.org/10.63125/2rpyze69

[35]. Mokhtari, A., Ahmadi, A., Daccache, A., & Drechsler, K. (2021). Actual evapotranspiration from UAV images: A multi-sensor data fusion approach. *Remote Sensing*, *13*(12), 2315. https://doi.org/10.3390/rs13122315

[36]. Olofsson, P., Foody, G. M., Herold, M., Stehman, S. V., Woodcock, C. E., & Wulder, M. A. (2014). Good practices for estimating area and assessing accuracy of land change. *Remote Sensing of Environment*, *148*, 42–57. https://doi.org/10.1016/j.rse.2014.02.015

[37]. Panagos, P., Borrelli, P., Poesen, J., Ballabio, C., Lugato, E., Meusburger, K., Montanarella, L., & Alewell, C. (2015). The new assessment of soil loss by water erosion in Europe. *Environmental Science & Policy*, *54*, 438–447. https://doi.org/10.1016/j.envsci.2015.08.012

[38]. Panahi, M., Gayen, A., & others. (2020). Flood susceptibility mapping using ensemble learning and GIS conditioning factors. *Science of the Total Environment*. https://doi.org/10.1016/j.scitotenv.2020.138845

[39]. Pourghasemi, H. R., Pouyan, S., Heidari, B., Farajzadeh, Z., Shamsi, S. R. F., Babaei, S., & Cerda, A. (2018). Spatial modeling, risk mapping, and validation of flood susceptibility using remote sensing and GIS. *Remote Sensing*, *10*(7), 1036. https://doi.org/10.3390/rs10071036

[40]. Rauf, M. A. (2018). A needs assessment approach to english for specific purposes (ESP) based syllabus design in Bangladesh vocational and technical education (BVTE). *International Journal of Educational Best Practices*, *2*(2), 18-25.

[41]. Rozenstein, O., Qin, Z., Derimian, Y., & Karnieli, A. (2014). Derivation of land surface temperature for Landsat-8 TIRS using a split window algorithm. *Sensors*, *14*(4), 5768–5780. https://doi.org/10.3390/s140405768

[42]. Sadeghi, M., Babaeian, E., Tuller, M., & Jones, S. B. (2017). The optical trapezoid model (rOPTRAM) for soil moisture estimation using optical remote sensing. *Remote Sensing of Environment*, *198*, 250–263. https://doi.org/10.1016/j.rse.2017.05.041

[43]. Sadeghi, M., Jones, S. B., & Babaeian, E. (2018). OPTRAM: A soil moisture retrieval algorithm using long-term MODIS observations. *Remote Sensing of Environment*, *211*, 425–440. https://doi.org/10.1016/j.rse.2018.04.029

[44]. Sai Praveen, K. (2024). AI-Enhanced Data Science Approaches For Optimizing User Engagement In U.S. Digital Marketing Campaigns. *Journal of Sustainable Development and Policy*, *3*(03), 01-43. https://doi.org/10.63125/65ebsn47

[45]. Santesteban, L. G., Di Gennaro, S. F., Herrero-Langreo, A., Miranda, C., Royo, J. B., & Matese, A. (2017). High-resolution UAV-based thermal imaging to estimate the instantaneous and seasonal variability of plant water status within a vineyard. *Agricultural Water Management*, *183*, 49–59. https://doi.org/10.1016/j.agwat.2016.08.026

[46]. Sepulcre-Cantó, G., Zarco-Tejada, P. J., & others. (2006). Detecting crop water stress by high-resolution thermal remote sensing. *Remote Sensing of Environment*. https://doi.org/10.1016/j.rse.2006.02.010

[47]. Shafizadeh-Moghadam, H., Valavi, R., Shahabi, H., Chapi, K., & Shirzadi, A. (2018). Novel forecasting approaches using combination of machine learning and statistical models for flood susceptibility mapping. *Journal of Environmental Management*, *217*, 1–11. https://doi.org/10.1016/j.jenvman.2018.03.089

[48]. Shoflul Azam, T., & Md. Al Amin, K. (2024). Quantitative Study on Machine Learning-Based Industrial Engineering Approaches For Reducing System Downtime In U.S. Manufacturing Plants. *International Journal of Scientific Interdisciplinary Research*, *5*(2), 526–558. https://doi.org/10.63125/kr9r1r90

[49]. Turner, D., Lucieer, A., & Watson, C. (2012). An automated technique for generating georectified mosaics from ultra-high resolution unmanned aerial vehicle (UAV) imagery, based on structure from motion (SfM) point clouds. *Remote Sensing*, *4*(5), 1392–1410. https://doi.org/10.3390/rs4051392

[50]. Valentin, C., Poesen, J., & Li, Y. (2005). Gully erosion: Impacts, factors and control. *Catena*, *63*(2–3), 132–153. https://doi.org/10.1016/j.catena.2005.06.001

[51]. Xu, X., Wang, Y., Li, J., & Zhao, Q. (2023). Spectral indices for tracing leaf water status with hyperspectral reflectance. *Journal of Applied Remote Sensing*, *17*(1), 014523. https://doi.org/10.1117/1.Jrs.17.014523

[52]. Yang, Y., Guan, H., Long, D., Liu, B., Qin, G., Qin, J., & Batelaan, O. (2015). Estimation of surface soil moisture from thermal infrared remote sensing using an improved trapezoid method. *Remote Sensing*, *7*(7), 8250–8270. https://doi.org/10.3390/rs70708250

[53]. Zaman, M. A. U., Sultana, S., Raju, V., & Rauf, M. A. (2021). Factors İmpacting the Uptake of İnnovative Open and Distance Learning (ODL) Programmes in Teacher Education. *Turkish Online Journal of Qualitative Inquiry*, *12*(6).

[54]. Zarco-Tejada, P. J., González-Dugo, V., & Berni, J. A. J. (2012). Fluorescence, temperature and narrow-band indices acquired from a UAV platform for water stress detection using a micro-hyperspectral imager and a thermal camera. *Remote Sensing of Environment*, *117*, 322–337. https://doi.org/10.1016/j.rse.2011.10.007

[55]. Zarco-Tejada, P. J., Suárez, L., & others. (2012). Hyperspectral and thermal retrievals for water stress quantification in orchards. *Remote Sensing of Environment*. https://doi.org/10.1016/j.rse.2012.01.020

[56]. Zhang, D., & Zhou, G. (2016). Estimation of soil moisture from optical and thermal remote sensing: A review. *Sensors*, *16*(8), 1308. https://doi.org/10.3390/s16081308

[57]. Zhang, F., & Zhou, G. (2019). Estimation of vegetation water content using hyperspectral vegetation indices: A comparison of crop water indicators in response to water stress treatments for summer maize. *BMC Ecology*, *19*, 18. https://doi.org/10.1186/s12898-019-0233-0

[58]. Zhang, J. (2010). Multi-source remote sensing data fusion: Status and trends. *International Journal of Image and Data Fusion*, *1*(1), 5–24. https://doi.org/10.1080/19479832.2010.523183

[59]. Zhang, L., Niu, Y., Zhang, H., Han, W., Li, G., Tang, J., & Peng, X. (2019). Maize canopy temperature extracted from UAV thermal and RGB imagery and its application in water stress monitoring. *Frontiers in Plant Science*, *10*, 1270. https://doi.org/10.3389/fpls.2019.01270

[60]. Zhao, W., Huang, J., Zhou, Q., & others. (2017). Hyperspectral characterization of soil moisture and salt stress (UAV/field scale). *Remote Sensing*, *9*(4), 317. https://doi.org/10.3390/rs9040317

[61]. Zurita-Milla, R., Laurent, V. C. E., & van Gijsel, J. A. E. (2015). Visualizing the ill-posedness of the inversion of a canopy radiative transfer model: A case study for Sentinel-2. *International Journal of Applied Earth Observation and Geoinformation*, *35*, 291–301. https://doi.org/10.1016/j.jag.2015.02.003